iScience

Article

Unraveling the structural and pigmentary mechanisms of UV color signal production in *Podarcis* wall lizards

Graphical abstract

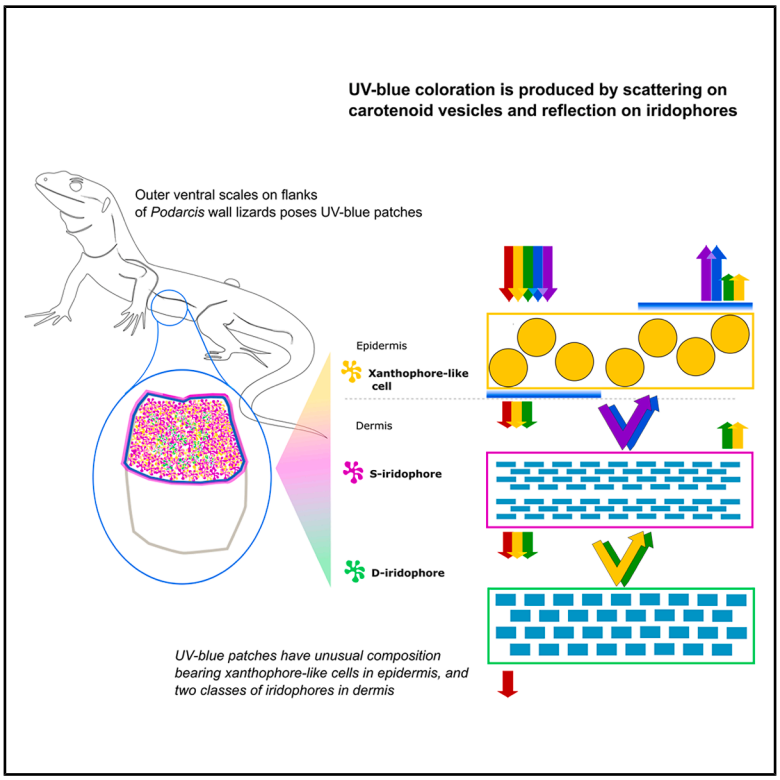

Highlights

- UV-blue patches of *Podarcis* lizards show unusual skin organization
- Epidermal carotenoid-containing cells interact with two dermal iridophore classes
- Yellow carotenoid vesicles enhance UV-blue reflectance through scattering
- Optical models show this mechanism expands the occupied color space

Authors

Jindřich Brejcha, Tomáš Ostatnický, Guillem Pérez i de Lanuza, ..., Jana Pilátová, Tatiana Vargicová, Enrique Font

Correspondence

brejcha@natur.cuni.cz

In brief

Animals; animal physiology; cellular physiology

Brejcha et al., 2026, iScience *29*, 116106
June 19, 2026
https://doi.org/10.1016/j.isci.2026.116106

CellPress

iScience

CellPress
OPEN ACCESS

Article

Unraveling the structural and pigmentary mechanisms of UV color signal production in *Podarcis* wall lizards

Jindřich Brejcha,[1,8,*] Tomáš Ostatnický,[2] Guillem Pérez i de Lanuza,[3] Peter Mojzeš,[4] Petr Maršík,[5] Jana Pilátová,[6] Tatiana Vargicová,[2] and Enrique Font[3,7]

[1]Department of Philosophy and History of Science, Faculty of Science, Charles University, 11636 Prague, Czech Republic
[2]Department of Chemical Physics and Optics, Faculty of Mathematics and Physics, Charles University, 11636 Prague, Czech Republic
[3]Ethology Lab, Cavanilles Institute of Biodiversity and Evolutionary Biology, University of Valencia, 46980 Paterna, València, Spain
[4]Institute of Physics of Charles University, Faculty of Mathematics and Physics, Charles University, 11636 Prague, Czech Republic
[5]Department of Food Science, Faculty of Agrobiology, Food and Natural Resources, Czech University of Life Sciences Prague, 59117 Prague, Czech Republic
[6]Molecular Foundry, Lawrence Berkeley National Laboratory, Berkeley, CA 94720, USA
[7]Senior author
[8]Lead contact
*Correspondence: brejcha@natur.cuni.cz
https://doi.org/10.1016/j.isci.2026.116106

SUMMARY

Color production in lizards has traditionally been explained by interactions among dermal chromatophores, yet the full diversity of coloration mechanisms remains incompletely understood. Additionally, while most studies focus on visible colors, UV reflectance plays a crucial role in lizard signaling and its mechanistic basis remains poorly characterized. Here, we investigate the UV-blue patches of *Podarcis* lizards. Using spectrophotometry, histology, electron microscopy, Raman spectroscopy, and optical modeling, we show that UV-blue coloration arises from interactions between carotenoid-containing epidermal xanthophore-like cells—an uncommon feature in vertebrate skin—and two morphologically distinct classes of iridophores. Superficial iridophores shape short-wavelength UV-blue reflectance, whereas deeper iridophores contribute to a secondary yellow-green peak. Although this mechanism is generalizable to other skin organizations, the UV-blue patches of *Podarcis* lizards exhibit a skin architecture not previously documented in vertebrates.

INTRODUCTION

Animal colors are among the most spectacular and diverse of phenotypic traits, playing important roles in thermoregulation, predator avoidance (e.g., camouflage and aposematism), and social communication.[1,2] Understanding this diversity requires knowledge of the mechanisms responsible for color production.[3] Reptiles in particular are highly colorful and their coloration is attracting increasing attention from researchers.[4] However, despite efforts over the past two decades,[5–7] the mechanisms underlying the production of reptile coloration remain only partially understood.

Color arises from the interaction of light with objects, which reflect a broad spectrum of wavelengths. In biological systems, the perceived color depends on the relative distribution of these reflected wavelengths, with the dominant range corresponding to the color observed. Colors may be either saturated (pure, characterized by a narrow range of reflected wavelengths) or desaturated, when reflectance is more broadly distributed, resulting in pastel or muted tones, or in extreme cases, an achromatic appearance such as gray or white. In reptiles, coloration is expressed primarily in the skin, where several mechanisms work in concert to produce the final appearance. Thus, reptile coloration can result from the absorption of light by pigment molecules (e.g., melanin, carotenoids, or pterins), from the interaction of light with nanometer-scale biological structures, and from a combination of both processes.[8]

Most studies of reptile coloration adhere to the dermal chromatophore unit concept.[9] Unlike mammals and birds, which typically have only one type of pigment cell in the epidermis, the skin of fish, amphibians, and non-avian reptiles contains several types of pigmentary and structural chromatophores, stacked within the dermis.[10] The primary chromatophore types are xanthophores, iridophores, and melanophores. These cells house color-producing elements (CPEs), i.e., morphological components that regulate light absorption, scattering, and reflection of incident light. In the case of chromatophores, the CPEs are intracellular organelles.[11] Xanthophores contain carotenoid vesicles or pterinosomes as their CPEs, those of iridophores are reflecting guanine platelets, and the CPEs of melanophores are melanosomes filled with melanin. As in the dermal chromatophore unit the chromatophores in reptile skin are

typically arranged in layers,[7,9] with xanthophores closest to the overlying epidermis, iridophores in an intermediate layer, and melanophores underneath. As an example of how chromatophores interact, the green coloration widely found in amphibians and reptiles is produced by blue light reflected by iridophores passing through overlying xanthophores, where yellow carotenoid vesicles filter the light.[12] However, the organization of chromatophores in the dermis varies, and one or more cell types can be absent or duplicated.[7] In some cases, iridophores occur in multiple layers or exist as two distinct classes (differing in the shape of their reflecting platelets) within a single-color patch; for instance, the discovery of superficial and deeper iridophore layers in panther chameleon skin has been highlighted as an evolutionary innovation linked to rapid color change.[13]

Many animal colors fall within the human visual range, but because many animals perceive colors differently from humans, some important colors remain undetectable by the human eye and require specialized equipment, such as spectrophotometry, for observation and measurement.[14] In the 1970s and 1980s, the recognition that non-human animals perceive colors differently spurred interest in the role of ultraviolet (UV) light in animal coloration, a research focus that continues today. Numerous studies have revealed that many species display color patches with reflectance peaks in the UV range (i.e., wavelengths below 400 nm). UV coloration is nearly ubiquitous in birds[15] and has been documented in fish, amphibians, and reptiles.[16] Given that many animals are capable of UV vision,[17] the presence of UV reflectance in skin color patches offers additional avenues for investigating chromatic signals and their underlying production mechanisms.

Shortwave reflectance such as UV (but also violet and blue) is most often of structural origin, produced by light scattering from CPEs in the tissues of the integument.[12] However, pigments can also contribute to blue coloration in certain cases.[18] Conversely, longwave reflectance (i.e., yellow and red) is typically pigment-based, resulting from selective light absorption by compounds such as carotenoids, pterins, or melanins, although structural mechanisms may sometimes contribute as well.[6,19–21] In pigment-based coloration, the absorption properties, concentration, and distribution of pigment compounds inside CPEs determine the final color.

In structural coloration, the key factors influencing color include the size, shape, and refractive index of the CPEs (i.e., scatterers), as well as their spatial arrangement.[22] The degree of organization of these CPEs determines whether the scattering is coherent or incoherent, an aspect that has received considerable attention in the biology of color.[23] In a coherent system, light waves scattered by different interfaces reinforce each other at specific wavelengths, producing distinct and intense colors. Incoherent scattering, on the other hand, causes light to be diffusely scattered across a broader range of wavelengths, resulting in less distinct coloration. The efficiency of scattering depends on the refractive index contrast between the CPEs and the surrounding medium, as well as the number and density of scattering interfaces. Highly saturated structural colors may require coherent scattering, where light interference amplifies certain wavelengths while minimizing others.[24] However, saturated colors can also arise from disordered structures, such as random assemblies of spherical nanoparticles that are all approximately the same size—comparable to the wavelengths of visible light.[25,26]

The nanoscale CPEs responsible for structural colors can be extracellular or intracellular. Extracellular CPEs, such as air-keratin-based or mucus-collagen-based matrices, are often involved in producing iridescent or non-iridescent colors in feathers, scales, and skin.[24] Among intracellular CPEs, the reflecting platelets within dermal iridophores are the best-known scatterers. Iridophores can function as broadband reflectors when their reflecting platelets are highly disorganized, producing desaturated colors, e.g., white, through incoherent scattering.[5] In contrast, when the platelets are well-organized, i.e., aligned in the same orientation and regularly spaced at distances comparable to the wavelengths of light, they generate reflectance through coherent scattering (i.e., constructive interference), amplifying specific wavelengths and producing saturated colors. Unlike reflecting platelets in iridophores, CPEs in xanthophores have not been seriously considered to produce color by scattering, even though similar structures make vivid colors in plants[27] and insects.[28]

Most lacertid lizards possess strongly UV-reflective patches on their flanks. In some species, these patches are visibly exposed all the time (e.g., *Timon Lepidus*[29] and *Gallotia galloti*[30]), whereas in others, such as most species in the genus *Podarcis*, they remain concealed in a resting posture and are actively displayed mainly during interactions with conspecifics. Motivated by the unusual appearance of these patches, we carried out a detailed examination to determine whether they differ structurally from the surrounding skin and how their color is produced. Here, we examine the skin of the European wall lizard, *Podarcis muralis* (Laurenti, 1768), a species with prominent UV-blue reflective patches, using spectrophotometry, histology, electron microscopy, and Raman microscopy. To place our findings in a broader comparative context, we also analyze the skin composition of two related species, *P. liolepis* (Boulanger, 1905) and *P. pityusensis* (Boscá, 1883).

Our results show that the UV-blue patches of *P. muralis* exhibit an unusual chromatophore organization that deviates from the classical dermal chromatophore unit concept. In particular, iridophores are divided into two distinct classes, differing in guanine crystal thickness, and there are carotenoid-containing cells unexpectedly abundant in the epidermis. The presence of epidermal xanthophore-like cells above iridophores is noteworthy, as yellow pigments, such as carotenoids, are typically expected to filter out short-wavelength reflectance. The presence of UV-blue coloration in these patches therefore raises questions about the optical interactions between pigmentary and structural components. The same chromatophore organization across multiple *Podarcis* species suggests that this arrangement is likely a shared trait of the lineage, offering new evolutionary insight into color production in these lizards.

RESULTS

The body surface of *Podarcis* lizards comprises multiple differently colored regions, each generated by its own local organization of skin chromatophores, yet the UV-blue flank patches stand

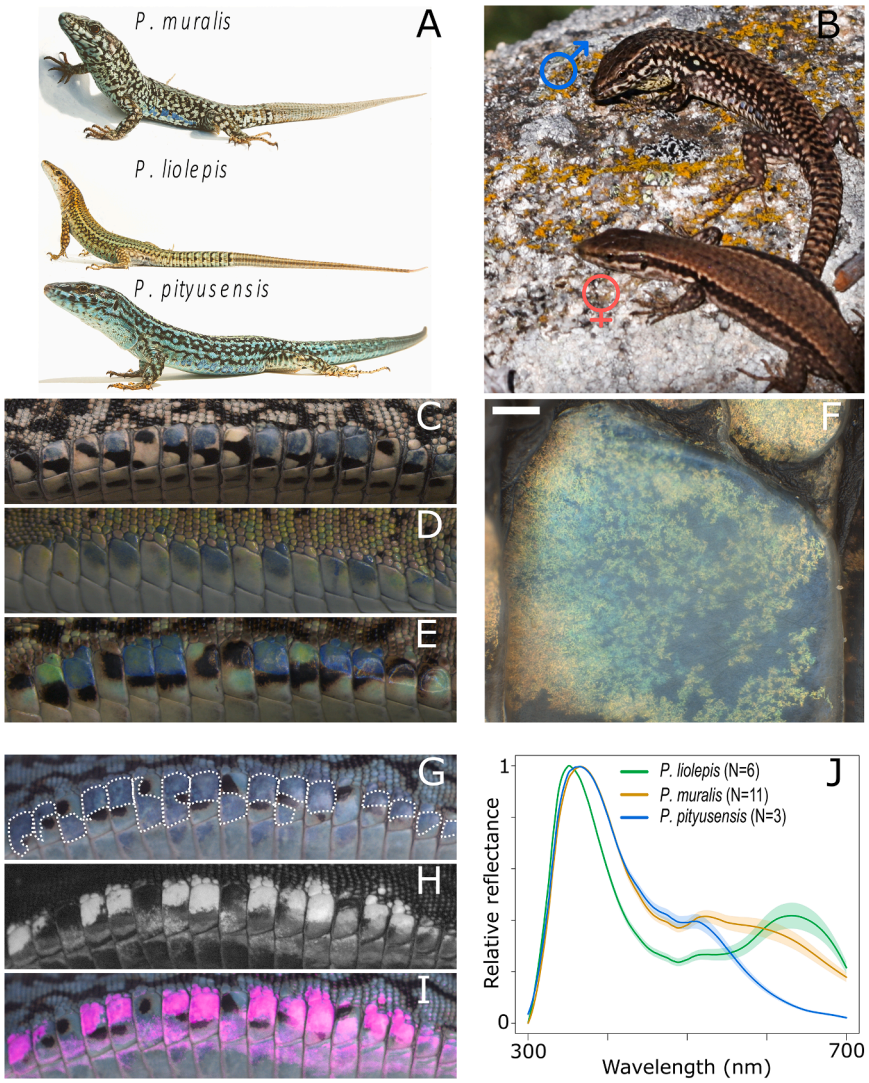

Figure 1. UV-blue patches are located on the ventrolateral body region, at the interface between ventral and dorsal scales

(A) All three studied *Podarcis* species: the European wall lizard (*P. muralis*), the brown wall lizard (*P. liolepis*), and the Ibiza wall lizard (*P. pityusensis*).

(B) A male of *P. muralis* in a typical hunched posture reveals UV-blue patches by flattening its body during an encounter with a female.

(C) UV-blue patches on the ventrolateral body region of the *P. muralis* in visible light.

(D) UV-blue patches on ventrolateral body region of *P. liolepis* in visible light.

(E) UV-blue patches on the ventrolateral body region of the green morph of *P. pityusensis* in visible light.

(F) Detail of UV-blue patch (*P. muralis*) under a binocular microscope in visible light. Scale bars, 200 μm.

(G) UV-blue patches (marked by dotted line) on the ventrolateral body region of the blue morph of the *P. pityusensis* in visible light.

(H) UV-blue patches on the ventrolateral body region of the blue morph of the *P. pityusensis* in UV light.

(I) UV-blue patches on the ventrolateral body region of the blue morph of the *P. pityusensis* with an overlay of visible (RGB channels) and UV (magenta channel) images.

(J) Reflectance spectra of three species of wall lizards (the lighter area around the curves indicates ±SEM). These spectra were obtained from individuals (*P. liolepis*—*N* = 6, *P. muralis*—*N* = 11, *P.pityusensis*—*N* = 3) captured for the purposes of this study, some of which were also used in subsequent experiments.

out as an especially conspicuous element of their color pattern.[31] Photographs of the three species studied here are presented in Figure 1A. Notably, lizards actively expose these patches during social interactions (Figure 1B), consistent with their signaling function (Figure 1B). Mostly rectangular or oval-shaped patches that look different shades of blue to the human eye are located in the ventrolateral regions of all three lizard species studied (*P. muralis*, *P. liolepis*, and *P. pityusensis*), often overlapping some of the outer ventral scales which mark the transition between the ventral (plate-like) and the lateral (granular) scales. The blue patches are irregularly spaced and separated by pale scales, which are usually the same color as the ventral scales but can sometimes appear greenish. Most scales in the ventrolateral region also have irregular black blotches, although the amount of black is highly variable (Figures 1C–1E). Upon closer magnification, the blue color appears as a hazy cloud on a background of black and light, yellow-green, cells (Figure 1F). UV photography shows that these blue patches reflect in the UV range, whereas the surrounding-colored regions usually do not. This holds true even for bluish individuals of *P. pityusensis*, where the bluish hue over the whole body does not reflect in the UV range (Figures 1G–1I). In reflectance spectra, the UV-blue patches exhibit a main peak in the near-UV range (approx. 370 nm), followed by a pronounced decline, often with a smaller secondary peak in the range from 500 to 700 nm (Figure 1J[32]).

The distribution of pigment cell types in dorsal and ventral skin of three species of *Podarcis* lizards

Although body coloration varies across regions outside the ventrolateral patches (Figure 2), all non-ventrolateral regions contain the same three dermal pigment cell types: xanthophores, iridophores, and melanophores.[32] These cells are characterized by their intracellular CPEs, including carotenoid vesicles (Figure 2A) and/or pterinosomes (Figure 2B) in xanthophores, reflecting platelets (Figure 2C) in iridophores, and melanosomes (Figure 2D) in melanophores. The content of dermal xanthophores in these regions is characteristically a mixture of carotenoid vesicles and pterinosomes (Figure 2E). The variability in the resulting surface color in regions other than the UV-blue patches is apparently determined by the

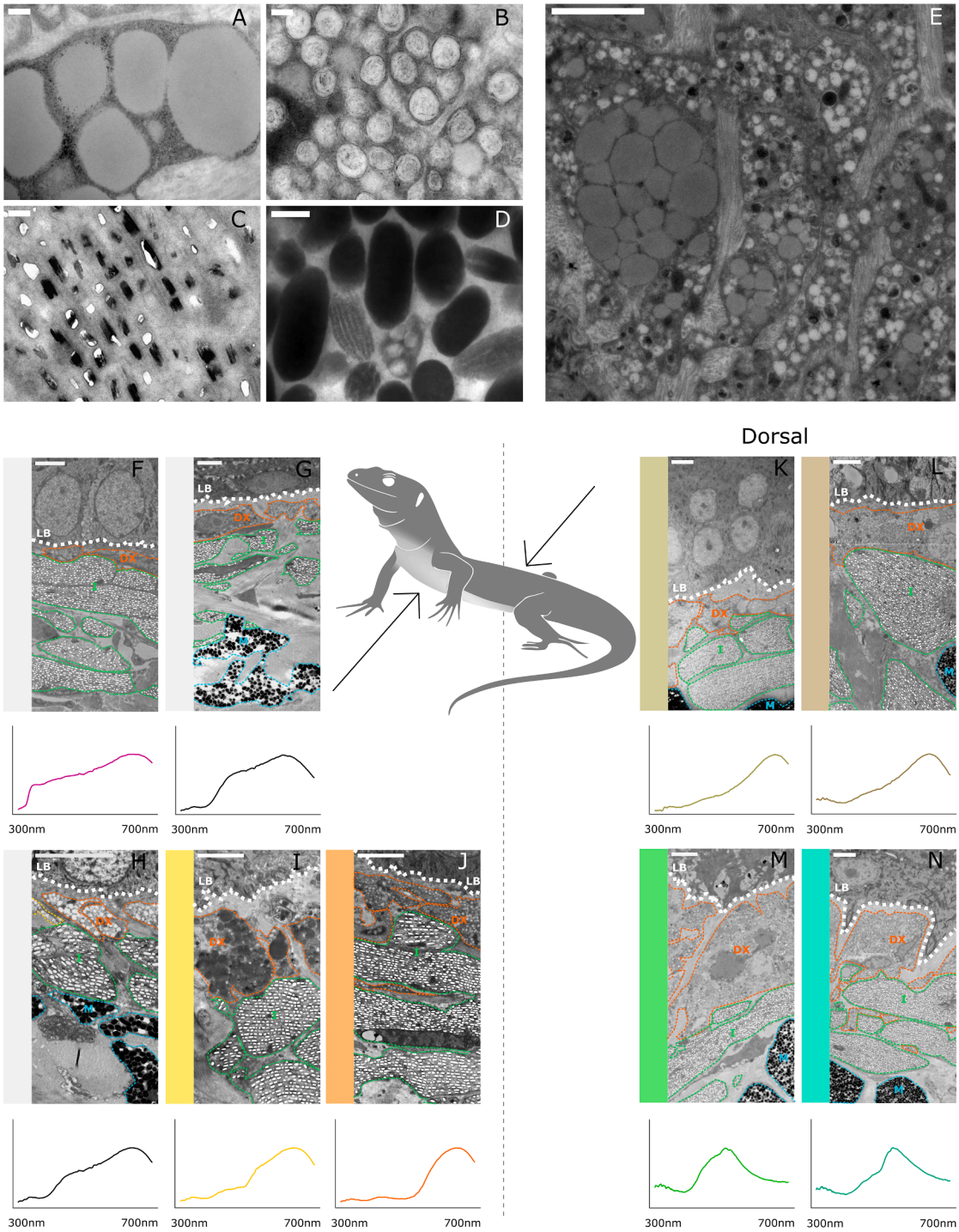

Figure 2. The distribution of pigment cell types in dorsal and ventral skin of three species *Podarcis* lizards

(A)–(D) show the CPEs in the skin of *Podarcis* lizards: (A) carotenoid vesicles, (B) pterinosomes, (C) reflecting platelets, and (D) melanosomes.

(E) Characteristic contents of dermal xanthophores in *Podarcis* lizards, consisting of a mixture of carotenoid vesicles, pterinosomes, and immature vesicles.

(F–N) show electron micrographs of lizard skin, where cell types were identified based on their CPEs. (F) White ventral scales of the brown wall lizard (*P. liolepis*). (G) White ventral scales of the Ibiza wall lizard (*P. pityusensis*). (H)–(J) show vVentral scales of the European wall lizard (*P. muralis*) in three different color morphs, which vary in xanthophore content: (H) the white morph contains a predominance of immature vesicles, (I) the yellow morph contains predominantly carotenoid vesicles, and (J) the orange morph contains primarily pterinosomes. (K) Brown dorsal scales of *P. liolepis*. (L) Brown dorsal scales of *P. muralis*. (M) and (N) display dorsal scales of *P. pityusensis*, which occur in two morphs: a green morph and a bluish morph, respectively.

(legend continued on next page)

thickness and content of individual layers of pigment cells (Figures 2F–2N). White regions in the throat and ventrum of many individuals contain a thin layer of dermal xanthophores, while yellow, orange, green, and bluish ventral and dorsal regions contain a thicker layer of xanthophores, which additionally feature prominent carotenoid vesicles (mean diameter = 333 nm, n = 711, SD = 220) and well-differentiated pterinosomes (mean diameter = 189 nm, n = 1,181, SD = 47). In dorsal and ventral skin, there is a single layer of iridophores. Reflecting platelets of the iridophore layer in ventral and dorsal skin appear well-organized, exhibiting a consistent shape of short rectangles. The arrangement of dermal pigment cells in all dorsal and ventral regions is consistent with the dermal chromatophore unit concept, with xanthophores predominantly located on the surface beneath the epidermis, followed by iridophores and, at the base, melanophores. None of the body regions, not even bluish dorsal coloration of *P. pityusensis*, shows spectral characteristics like the UV-blue patches located on the flanks (Figures 2F–2N).

UV-blue patches contain epidermal xanthophore-like cells and two types of iridophores

When compared to other skin regions, the ventrolateral UV-blue patches differ in their composition, as they contain four pigment cell phenotypes: xanthophore-like cells, more superficial and deeper iridophores, and melanophores (Figure 3[32]). The epidermis and dermis in the UV-blue patches are separated by a prominent basal lamina (Figures 3A and 3B), which is underlined with thin dermal collagenous lamella. The basal lamina was identified in TEM sections as a very thin continuous, uniformly electron-dense layer underlying basal keratinocytes. In the epidermis of the UV-blue patches, we found cells bearing spherical structures that resemble carotenoid-containing vesicles of xanthophores (Figures 3A–3C). These vesicles are similar in size and have a mean diameter of 460 nm (n = 4,929, SD = 241 nm) (Figure 8B). The abundant epidermal xanthophore-like cells are distributed within the basal layer of keratinocytes (Figures 3A–3C), and extent over the entire area of the UV-blue patch (Figure S1).

In the dermis of the UV-blue patches we found iridophores underlain by dermal melanophores, but no ordinary dermal xanthophores (Figure 3). Noticeably, the iridophores in the UV-blue patches are arranged in two layers differing in the size and shape of their crystals (Figures 3A and 3D). We call more superficially located iridophores S-iridophores (Figures 3A and 3D), and a second layer located deeper in the dermis D-iridophores (Figures 3A and 3D). We chose this terminology because it accurately describes the characteristic arrangement of the two classes of iridophores in the dermis relative to the skin surface. However, it is important to emphasize that it is by no means intended to imply any homology with the S- and D-iridophores described in chameleons,[13] nor the lack thereof. Reflecting platelets in S-iridophores are thin and elongated, appearing needle-like in cross-section, whereas the crystals in D-iridophores are thicker but shorter, giving them a rectangular appearance in cross-section (Figures 3D and 8A). The thickness of platelets differs significantly between the iridophore types (estimate = −34, SE = 1.65, t = −20.71, $p < 0.01$) with S-iridophores having 44 nm thick (n = 411, SD = 17 nm), and D-iridophores with 79 nm thick platelets (n = 607, SD = 31 nm) (Figure 8B). The D-iridophores resemble the iridophore layer found outside the ventrolateral UV-blue patches in terms of crystal morphology, whereas the superficial S-iridophores appear to be a derived and are only found in UV-blue patches.

In both iridophore populations, the reflecting platelets appear to be well-organized and are arranged roughly parallel to the skin surface. S-iridophores are typically the most prominent in terms of layer thickness in the dermis of the UV-blue patches, relative to D-iridophores. In areas where blue transitions to black, S-iridophores extend as a thin layer into the margins of the black regions. D-iridophores never extend into the black regions, but sometimes they may occur without S-iridophores in blue areas. This suggests that in blue areas, D-iridophores create a light background, whereas in dark areas, whether deep blue or black, the background color is due to the underlying melanophores. Where S-iridophores are present, epidermal xanthophore-like cells are always found above them, varying in number and distribution, even in marginal areas where blue gradually transitions to black. This suggests that the S-iridophores contribute to the UV-blue color together with epidermal xanthophores. The ventrolateral UV-blue patches of all three studied species show the same unique cellular composition (Figure 4[32]).

In contrast to the UV-blue patches, the non-UV-blue pale parts of the ventrolateral region have a pigment cell composition similar to the skin in other regions of the lizards' bodies. Their xanthophores are in the dermis and contain a mixture of pterinosomes and/or carotenoid vesicles (Figures 5A–5C[32]). We observed an epidermal xanthophore-like cell in the non-UV-blue ventrolateral region only once, and in that case an S-iridophore was also present in the dermis (Figure 5D).

We occasionally found individual xanthophores apparently protruding into the epidermis through the basal lamina in dorsal and ventral skin (Figures 5E–5G). Notably, in both the dorsal and ventral regions, these xanthophores protruding into the epidermis were not accompanied by S-iridophores. This suggests that S-iridophores are restricted to ventrolateral scales, whereas individual instances of xanthophores protruding across the basal lamina can occur in other body regions.

It was sometimes unclear whether the xanthophores protruding into epidermis originated in the dermis, with the basal lamina separating them from the epidermis, or they were actually fully within the epidermis outside the ventrolateral region

In all images, pigment cell types are consistently marked as follows: dermal xanthophores (DX, orange), iridophores (I, green), and melanophores (M, turquoise). Pigment cells are located in the dermis below the basal lamina (LB, dashed white line), which separates them from the epidermis above. The vertical color bars adjacent to the TEM images indicate the approximate coloration of each region; however, they are illustrative and do not reflect exact hues. The graphs below TEM images show standardized reflectance spectra of the corresponding regions. Scale bars: 200 nm in (A)–(D), 2 μm in (E), and 3 μm in (F)–(N). Eleven males of *P. muralis*, 1 male of *P. liolepis*, and 2 males of *P. pityusensis* were examined.

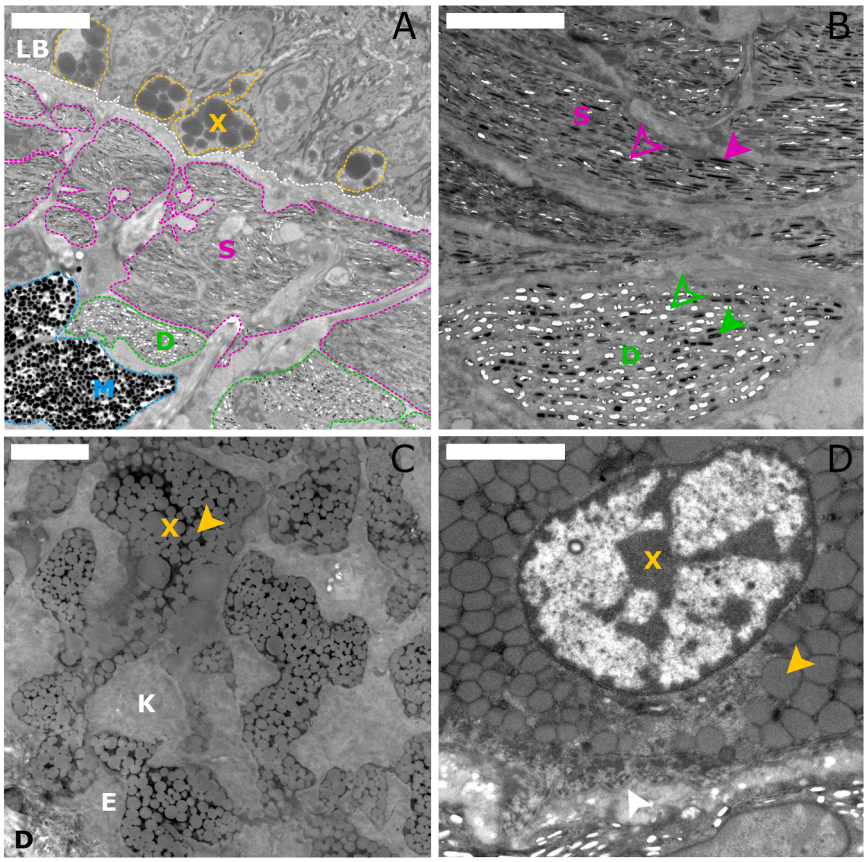

Figure 3. Cellular composition of the UV-blue patches of the European wall lizard (*P. muralis*)

(A) Cross-section through the UV-blue ventrolateral patch. The basal lamina (LB; white dashed line) separates the epidermis (above) from the dermis (below). The epidermis contains xanthophore-like cells (X; yellow) filled with spherical droplets resembling carotenoid vesicles. Within the dermis, two layers of iridophores are visible: S-iridophores (S; magenta) located immediately below the basal lamina, and D-iridophores (D; green) positioned deeper in the skin. At the margin of the image, a melanophore (M; blue) extends upward between the D-iridophore layer. Scale bars, 5 μm.

(B) Detail of both iridophore classes. S-iridophore (S; magenta) and D-iridophore (D; green). Arrowheads indicate differences between intact guanine crystals (filled arrowheads) and empty spaces remaining after crystal loss (open arrowheads). Scale bars, 2 μm.

(C) Longitudinal section of the epidermis (E) showing abundant xanthophore-like cells (X; yellow) within the basal layer of keratinocytes (K). The lower left corner reveals part of the dermis due to a slightly oblique section. A yellow arrowhead indicates a vesicle within a xanthophore-like cell. Scale bars, 5 μm.

(D) Detail of a xanthophore-like cell (X; yellow) with a visible nucleus and numerous carotenoid vesicles (yellow arrowhead). The white arrowhead marks the basal lamina, clearly separating the cell from the dermis. Scale bars, 2 μm. See also Figure S1. Eleven males of *P. muralis* were examined.

(Figures 5E–5G). In contrast, in the UV-blue patches of the ventrolateral region, epidermal xanthophore-like cells are, as a rule, clearly separated from the dermis by a basal lamina (Figure 3B). Nevertheless, although rare, xanthophore-like cells in the UV-blue patches can also appear on both sides of the basal lamina, that is, both in the dermis and in the epidermis (Figure 5H).

Figure 6 depicts summary of the composition of different skin regions of *Podarcis* lizards.

Epidermal xanthophore-like cells contain yellow carotenoid pigment

To characterize in more detail the contents of epidermal xanthophore-like cells, we first observed unstained cryosections and found that they contain yellow vesicles (Figure 7A) that show autofluorescence in green after excitation by blue light (Figure 7B). Such an autofluorescence pattern suggests that the vesicles contain carotenoids.[33,34] Sudan-black staining confirmed the presence of lipid contents in the epidermal xanthophore-like cells (Figure 7C). Based on their characteristic absorbance spectrum, HPLC indicated the presence of carotenoids in the ventrolateral region of the lizard skin (Figure 7D[32]). Our previous analyses found lutein and zeaxanthin to be responsible for the yellow color in ventral skin of *P. muralis*.[35] Thus, it is possible that those same carotenoids are also present in the vesicles of epidermal xanthophore-like cells. However, some shortcomings in our methodology need to be considered. First, our results do not clarify whether the carotenoids are confined to the UV-blue patches or are found throughout the tissue. This could be addressed by isolating and extracting carotenoids only from the blue parts of the scales. However, this approach results in the loss of focal tissue, which is already limited. The second drawback is connected to this issue. Due to the limited amount of tissue, especially because the UV-blue patches occupy only a small part of the entire ventrolateral region, the resulting concentration of extract is rather poor. This leads to a rather weak PDA signal, and the measured absorbance of focal substances barely stands out on the chromatogram above background level (Figure S2). To increase the extract concentration, itwould be necessary to do extractions based on skin samples from many individuals, which is ethically problematic.

Hence, for a finer determination and localization of carotenoids in the UV-blue patches, we opted for the sensitive method of confocal Raman microscopy. Raman microscopy results demonstrate clearly the presence of carotenoids in the UV-blue patches (Figures 7E, 7F, 7I, and S4[32]). The results also indicate that the epidermis is primarily composed of keratin (Figures 7E, 7I, and S5), but it seems that the basal layer

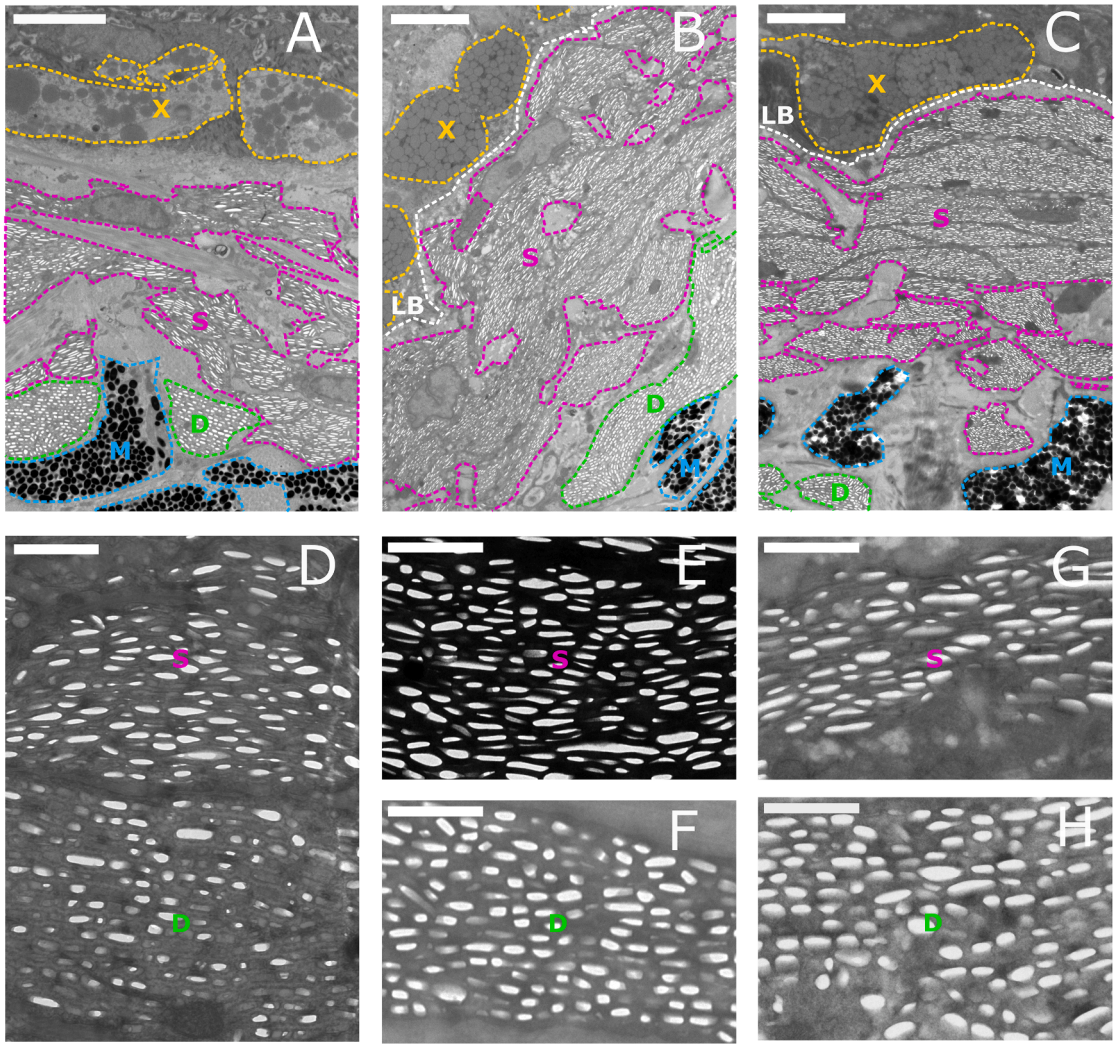

Figure 4. UV-blue patches of three *Podarcis* lizard species

(A–C) Overview of the cellular composition of UV-blue patches in the three studied lizard species. (A) European wall lizard (*P. muralis*), (B) brown wall lizard (*P. liolepis*), and (C) Ibiza wall lizard (*P. pityusensis*). Epidermal xanthophore-like cells (X, yellow), S-iridophores (S, magenta), D-iridophores (D, green), melanophores (M, blue), and basal lamina (LB, dashed white line). Scale bars, 5 μm.

(D–H) Detail of individual classes of iridophores. All images show empty spaces remaining after crystal loss during sample preparation. Scale bars, 1 μm. (D) S- and D-iridophores of *P. muralis*. (E) S-iridophores of *P. liolepis*. (F) D-iridophores of *P. liolepis*. (G) S-iridophores of *P. pityusensis*. (H) D-iridophores of *P. pityusensis*. Eleven males of *P. muralis*, 1 male of *P. liolepis*, and 2 males of *P. pityusensis* were examined.

of the epidermis, where xanthophore-like cells are located, is probably not rich in keratin. Raman microscopy also shows that the reflecting platelets of iridophores are composed of guanine (Figures 7E, 7G, 7I, and S5). However, we did not detect any differences in the composition of the two layers of iridophores. Raman microscopy also revealed that the pigment in the melanophores of the UV-blue patches is primarily eumelanin (Figures 7E, 7H, 7I, and S5). Raman microscopy complements our observation-based hypothesis that the presence of carotenoid-containing cells is characteristic for the UV-blue patches of the ventrolateral region and that the cells containing these carotenoids densely cover the UV-blue patches across their entire surface (Figure S6).

Models of UV-blue color production suggest close interplay of reflectance on iridophores and scattering by carotenoid vesicles

Dimensions of the carotenoid vesicles in epidermal xanthophore-like cells, reflecting platelets of both iridophore populations and their spacing (mean spacing 76 nm for S-iridophores, SD = 97 nm, and 115 nm for D-iridophores, SD = 145 nm) as measured from TEM are shown in Figures 8A and 8B (see also Figure S7[32]). As structural colors in lizards have been primarily attributed to iridophore reflecting platelets, we first modeled the reflectance from regularly distributed reflecting platelets in S- and D-iridophores as a layered medium. The results show that S-iridophores reflect predominantly in the UV-blue part of the spectrum, while D-iridophores reflect mainly in the

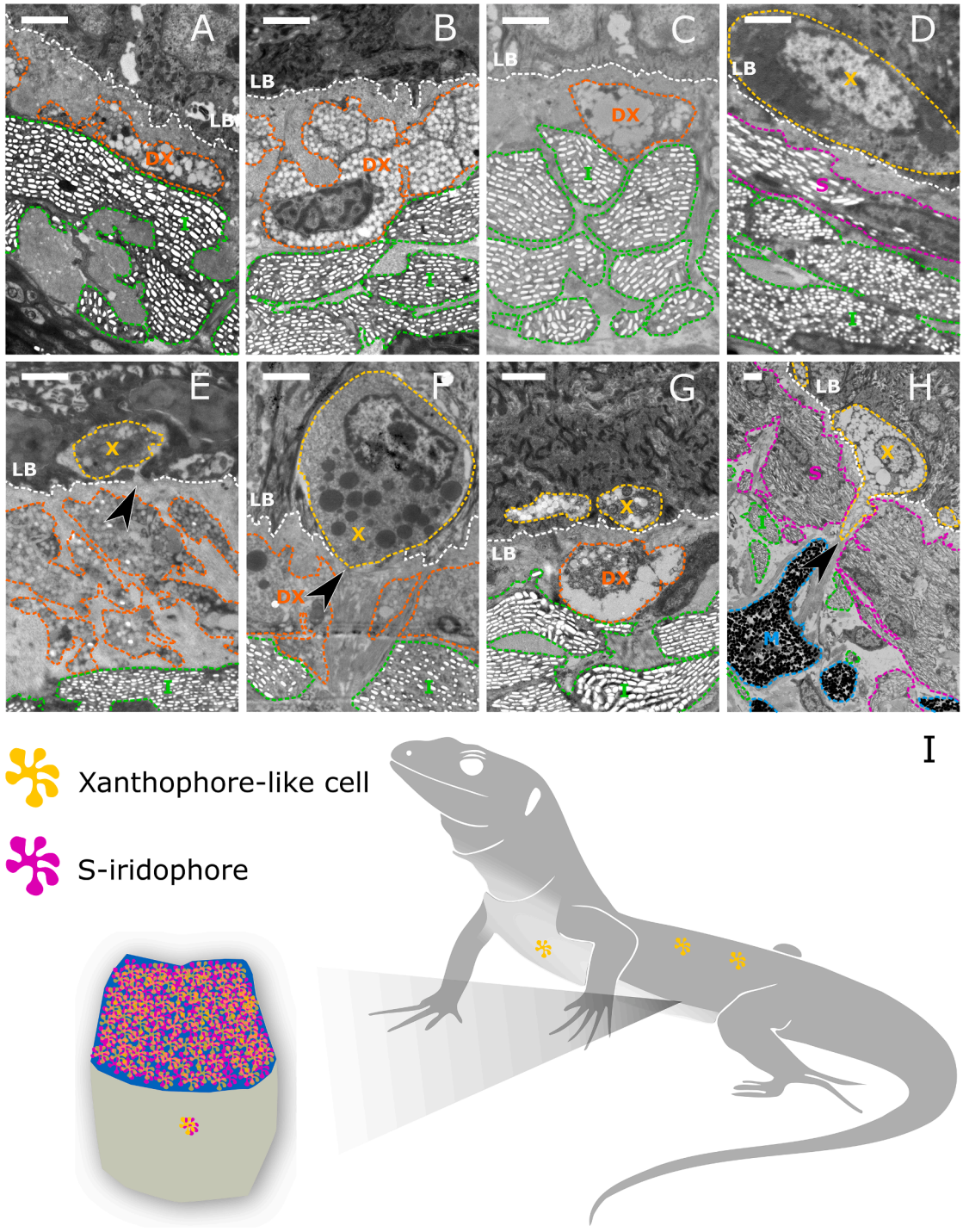

Figure 5. Cellular composition of non-UV-blue parts of the ventrolateral region, and exceptional cases outside of the ventrolateral region

(A) Non-UV non-blue part of the ventrolateral region the European wall lizard (*Podarcis muralis*).

(B) Non-UV non-blue part of the ventrolateral region in the Ibiza wall lizard (*P. pityusensis*).

(C) Non-UV non-blue part of the ventrolateral region in the brown wall lizard (*P. liolepis*). Please note the enlarged carotenoid vesicles inside xanthophores compared to mostly smaller pterinosomes of xanthophores in (A).

(D) Exceptional case where non-UV non-blue part of the ventrolateral region contains both epidermal xanthophore-like cell and S-iridophore, here in *P. muralis*. Notably, both cell types appear together.

(legend continued on next page)

green-yellow part of the spectrum (Figure 8C). However, neither the predicted spectrum of the S-iridophores nor that of the D-iridophores matches the observed reflectance pattern, and even their combined contribution produces a spectrum that is too flat to account for the sharp UV-blue peak seen in the spectrophotometric measurements (compare Figure 8C with Figure 1J). This discrepancy is further complicated by the fact that the iridophores are overlain by a layer of epidermal xanthophore-like cells. Therefore, we then tested whether the observed UV-blue color could result from a combination of reflection by guanine platelets of iridophores and Mie scattering by carotenoid vesicles in epidermal xanthophore-like cells (for justification of the theoretical bases for this model see supplemental results in Figure S8).

Published theoretical models suggest that scattering efficiency should be highest in forward directions, while backscattering should remain low (cf. Figure 4.9 in Bohren and Huffman[36]). Our calculations confirm that, given the parameters used and random distribution of carotenoid vesicles, backscattering cancels out (Figure S8). As a result, forward scattering remains the dominant contribution, with backscattering being orders of magnitude weaker.

Spectra of the total scattering efficiency by carotenoid vesicles are shown in Figure 8D for several values of the carotenoid vesicles' intrinsic refractive index N_0 and its peak absorption coefficient (since these values have not been determined experimentally). Modeled spectra reveal an absorption band between 400 and 500 nm due to the presence of the carotenoid pigment (Figure 8D). Preferential scattering in the short-wavelength part of the spectrum is predicted for all droplet refractive indexes, independently of the peak absorption.

Combining the results of modeling reflecting platelets and carotenoid vesicles, we obtained a reflectance spectrum (the $2I_1(\lambda)$, sum of the paths 1 and 2, see "STAR Methods" for further details and Figure S9) similar to the measured reflectance of the UV-blue patches. Although this approach takes into account the contribution of epidermal xanthophore-like cells to color production, the model still does not predict a drop in reflectance near 300 nm. This is because, based on the dimensions of the reflecting platelets in the S-iridophores, the model anticipates a continuous increase in reflectance up to just below 300 nm and the same applies to the scattering efficiency of carotenoid vesicles in epidermal xanthophore-like cells (compare spectra in Figures 8C and 8D). To account for this discrepancy, we introduced an additional absorbing component to simulate the drop in reflectance below 300 nm. One possible candidate is keratin, whose published absorption spectrum overlaps this region.[37] The resulting spectra, accounting for the interplay between xanthophores, iridophores and short-wavelength absorption, are shown in Figure 8E.

Results also show the dependence of blue color production on the size of the carotenoid vesicles and their refractive index. In Figure 8F, we show calculated dependency of the produced spectrum displayed in real colors (RGB) on refractive index (the N_0) of carotenoid vesicles and their radius. It is established that the refractive index of compounds increases with concentration.[38,39] The results indicate that for carotenoid vesicle sizes up to 400 nm, the predicted color is UV-blue regardless of the concentration of carotenoids. However, for sizes of carotenoid vesicles ranging from 400 to 600 nm, the predicted color is yellow to white, depending on the concentration of carotenoids. For carotenoid vesicle sizes from 600 to 1000 nm, lower concentrations of carotenoids predict the production of a yellow color, but with increasing concentrations of carotenoids, the production of blue color may occur.

Evaluating model fit to measured UV-blue patch reflectance and its intraspecific variation

To assess how well our approach matches empirical measurements and to compare its performance with an established modeling framework, we examined its behavior under variation in selected parameters (Figure 9; see STAR Methods for further details). We evaluated three modeling approaches. In the standard "filter" model, xanthophores are represented as a continuous layer of absorptive pigment medium overlying the iridophores. In the enhanced "scatterers" model, xanthophores are additionally treated as randomly distributed, pigment-containing scatterers embedded above the iridophores, yet still absorbing a part of incoming light and thus acting as spectral filters. Finally, the "mosaic" model accounts for the heterogeneous nature of UV-blue patches by combining spectra generated from multiple local micro-configurations within a single color patch. The modeling resulted in 4,742 spectra (2,305 spectra for the standard "filter" model, 2,305 spectra for the "scatterers" model, and 132 spectra for the "mosaic" model[32]). These theoretical spectra were compared to 541 empirical reflectance spectra of real UV-blue patches of male *P. muralis*.

(E) Individual case of a dorsal scale of bluish morph of *P. pityusensis* containing a xanthophore-like cell seemingly protruding into the epidermis. Note the shape of basal lamina in place of protrusion (arrowhead). Compared to typical xanthophore like cells in the UV blue patch of ventrolateral region this cell does not contain large carotenoid vesicles, and the putative evagination involves the extracellular space.
(F) Exceptional case of dorsal scale of *P. muralis* containing xanthophore-like cell that seems to be migrating into the epidermis. Note bundles of collagen oriented perpendicular to the area of the disrupted basal lamina (arrowhead) at the base of the xanthophore cell.
(G) Exceptional case of ventral scale of white morph of *P. muralis* containing xanthophore-like cell in the epidermis.
(H) Putative migrating xanthophore-like cell in the UV-blue ventrolateral patches. Note the shape of the cell together with collagen bundles perpendicularly oriented toward disrupted lamina basal (arrowhead).
(I) Schematic summary of epidermal xanthophore-like cell occurrence. Within the UV-blue ventrolateral region, the presence of epidermal xanthophore-like cells together with S-iridophores constitutes the rule. Other observations, whether the simultaneous presence of epidermal xanthophore-like cells and S-iridophores, or the occurrence of epidermal xanthophore-like cells alone, represent isolated occurrences, as illustrated in the schematic. Xanthophore-like cells that occur in epidermis (X, yellow), dermal xanthophores (DX, orange), S-iridophores (S, magenta), D-iridophores (D, green), and melanophores (M, cyan). The white dashed line indicates the basal lamina (LB). Scale bars, 2 μm for all images in the figure. Eleven males of *P. muralis*, 1 male of *P. liolepis*, and 2 males of *P. pityusensis* were examined.

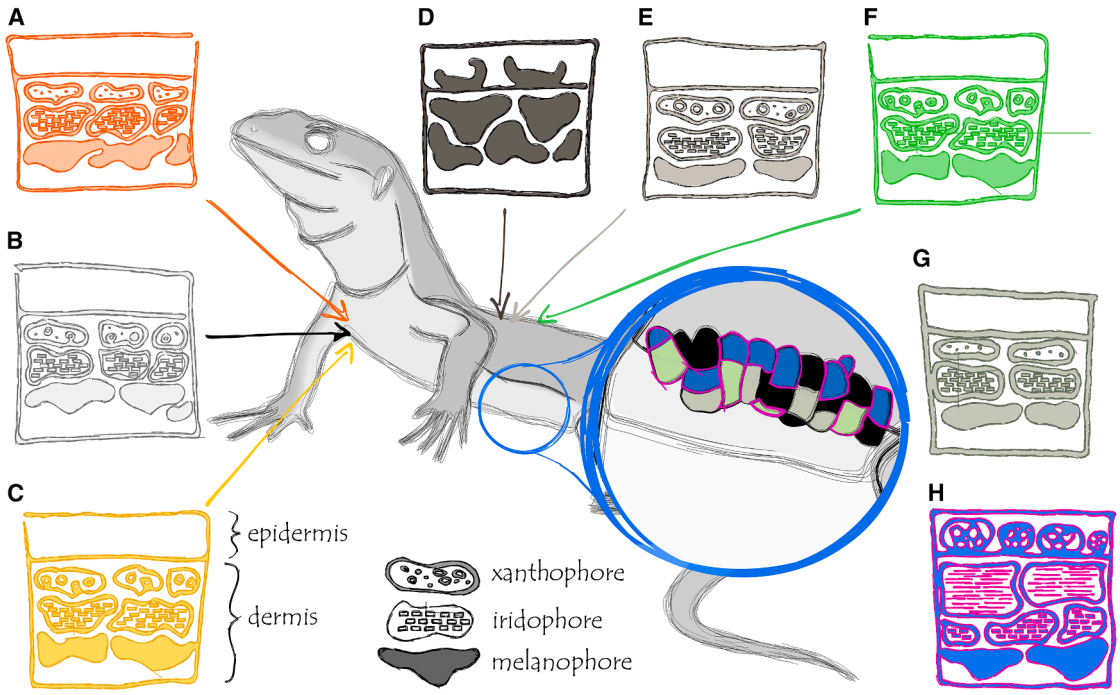

Figure 6. Schematic representation of chromatophore organization across different color regions of *Podarcis* lizards

The central illustration shows a generalized *Podarcis* lizard in grayscale with arrows pointing to body regions corresponding to eight sampled skin regions. (A–H) Rectangles depict idealized vertical sections through the skin, illustrating the relative arrangement of chromatophores in each region. The three main chromatophore types (xanthophores, iridophores, and melanophores) are shown as layered components of the dermis. (A) Orange ventral region, characterized by xanthophores with abundant pterinosomes, organized reflecting platelets in iridophores, and underlying melanocytes. (B) White ventral region, similar in structure to A, but the vesicles inside xanthophores include a mixture of pterinosomes and carotenoid vesicles. (C) Yellow ventral region, comparable to (A) and (B), but with xanthophores predominantly containing carotenoid vesicles. (D) Black dorsal region, characterized by the presence of both epidermal and dermal melanocytes, and the absence of xanthophores and iridophores. (E) Light dorsal region, containing dermal xanthophores, iridophores, and underlying melanocytes, organized similarly to the ventral regions. (F) Vivid green dorsal region, marked by an abundance of xanthophores packed with carotenoid vesicles, overlying dermal iridophores and melanocytes as in the ventral regions. (G) Non-UV-reflective ventrolateral patches, similar to ventral regions, with dermal xanthophores containing a mix of carotenoid vesicles and pterinosomes, along with iridophores and melanocytes. (H) UV-blue ventrolateral patches, which are distinct in having xanthophore-like cells packed with carotenoid vesicles in the epidermis, as well as two types of iridophores: superficial S-iridophores with thin, elongated reflecting platelets, and deeper D-iridophores with shorter but thicker platelets located just above a layer of melanocytes in the dermis. Cell types are denoted by their contents: xanthophores with circular inclusions, iridophores with brick-like platelet arrays, and melanocytes as a solid black layer. Colors in the figure are illustrative and do not represent exact hues.

All modeled and measured spectra projected into a color tetrahedron that represents *Podarcis* perceptual color space are depicted in Figure 9A. The convex-hull volumes that these spectra occupy in the lizard's visual color space are shown in Figure 9B. To assess the fit of the "filter" and "scatterers" models, we calculated the overlap between the volume occupied in tetrahedral color space by each model and measured reflectance data. The "filter" model-generated spectra occupy a smaller volume (3.38×10^{-5}) compared to the measured reflectance spectra of UV-blue patches of lizards (2×10^{-4}), while the "scatterers" model spectra occupy a larger volume (1.50×10^{-3}). Overlap between these volumes in lizard color-space provides a measure of how well the modeled spectra match the empirical data; overlap is expressed either relative to the smaller volume (vsmallest, indicating containment) or relative to the total combined volume (vboth, indicating overall similarity). The overlap of the "filter" model with the measured data is clearly lower (vsmallest = 3.67×10^{-3}; vboth = 4.21×10^{-4}) than the overlap of measured data with the "scatterers" model outputs (vsmallest = 2.54×10^{-1}; vboth = 3.91×10^{-2}). Additionally, the volume generated by the proposed "scatterers" model encompasses almost all the data produced by the existing "filter" model (vsmallest = 9.99×10^{-1}; vboth = 2.25×10^{-2}). The low vboth values in comparisons involving the "scatterers" model reflect its substantially larger occupied color-volume rather than poor correspondence with the empirical data. Notably, the "scatterers" model subsumes the range of color space predicted by the "filter" model while extending beyond it.

Although the spectra produced by the "scatterers" model better fit real spectral data, they still do not cover the volume of real data extending from the achromatic point toward the UV region (Figures 9A and 9B). This is especially true for the part of the UV volume influenced by the yellow-red wavelengths of the spectrum, which may be attributed to variations in the secondary peak of the real reflectance spectrum of the UV-blue patches (Figure 9C). According to predictions for individual cell types, this variation could be explained by the influence of D-iridophores compared to the effect of

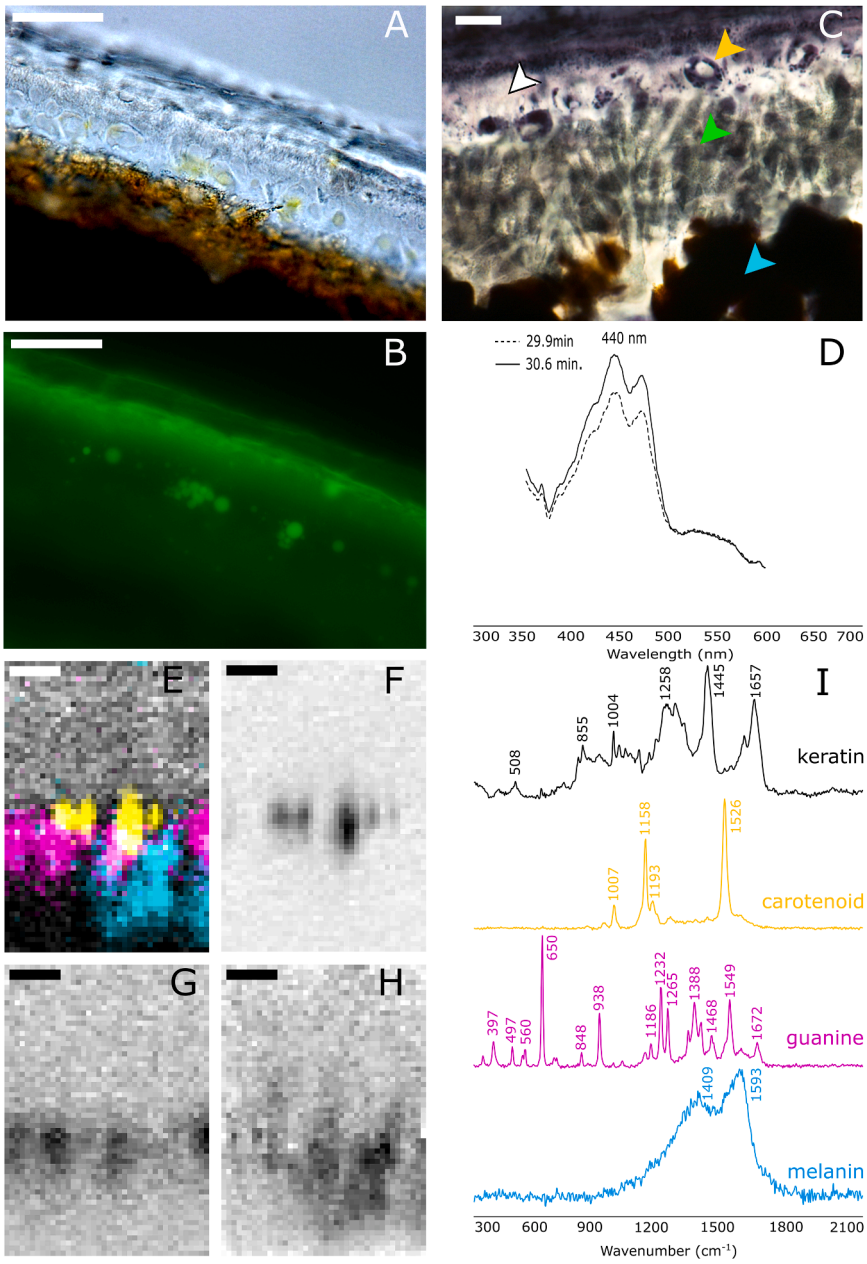

Figure 7. Epidermal xanthophore-like cells contain yellow carotenoid pigment

(A and B) Light microscopy (LM): (A) brightfield LM of an unstained cryosection (15 μm thick) through the UV-blue patch of the European wall lizard (*Podarcis muralis*) showing yellow vesicles in the transparent epidermis, underlined by brown looking iridophores and black melanophores. (B) Same cryosection as in (A) after excitation by a 488 nm light source showing auto-fluorescence, appearing green under the LM due to the 566 nm long-pass filter in the emission path. Note that the vesicles that appear yellow in (A), fluoresce, which may suggest presence of carotenoid pigments.

(C) Sudan black stained cryosection. White arrowhead shows epidermis, yellow xanthophore-like cells with stained lipid vesicles, green iridophores, and cyan melanophores.

(D) PDA detected absorbance spectra of the two extracted compound from the ventrolateral region showing the characteristic shape of yellow carotenoids with λ max = 440 nm.

(E–H) Confocal Raman microscopy (CRM) results of depth scan through the UV-blue patch of *P. muralis* depicted as map of the Raman signal from the tissue. (E) Composition image mapping signals of various compounds detected. Most superficially in gray is the epidermis containing keratin. Directly adjacent to the epidermis is a layer of xanthophore-like cells containing carotenoids (yellow). The xanthophore-like cells are underlain by iridophores containing guanine (magenta), and deepest lie melanophores containing melanin (cyan). (F) CRM spatially mapped carotenoid signals (black). (G) CRM spatially mapped signal of guanine (black). (H) CRM spatially mapped signal of melanin (black).

(I) Raman spectra characterizing the depicted compounds measured in the UV-blue patch. From the top to the bottom: Raman spectrum of keratin (black), carotenoid (yellow), guanine (magenta), and melanin (cyan). For a comparison between spectra measured in the UV-blue patch and the corresponding reference spectra, compare with Figures S4 and S5. Scale bars: 25 μm in (A) and (B), 10 μm in (D), and 5 μm in (E)–(H). See also Figures S2–S6. Five males of *P. muralis*, 1 male of *P. liolepis*, and 1 male of *P. pityusensis* were examined.

interactions between epidermal xanthophore-like cells and S-iridophores.

Given that the tissue is not homogeneous in terms of cellular composition at the microscopic level within the UV-blue patch, we modeled a scenario where the tissue is composed of a "mosaic" of cells (Figure 9F) with varying percentage coverage. The "mosaic" model (Figure 9D, gray points in Figure 9A) successfully simulated spectra that extend significantly far into the UV region and cover the color space observed in real measurements, reaching areas that the basic "scatterers" model did not. Furthermore, a visual comparison of the variability in the shape of real reflectance spectra of UV-blue patches (Figure 9C) and the spectra from the "mosaic" model (Figure 9D) shows a good fit. The variability in UV-blue spectra of ventrolateral region within the lizard population may, therefore, be influenced by factors other than CPEs' geometry or pigment concentration, such as the coverage within the color patch by different types of pigment cells on a microscopic scale.

DISCUSSION

In *Podarcis* lizards, we identify a previously unrecognized mechanism of UV-blue color production, characterized by the

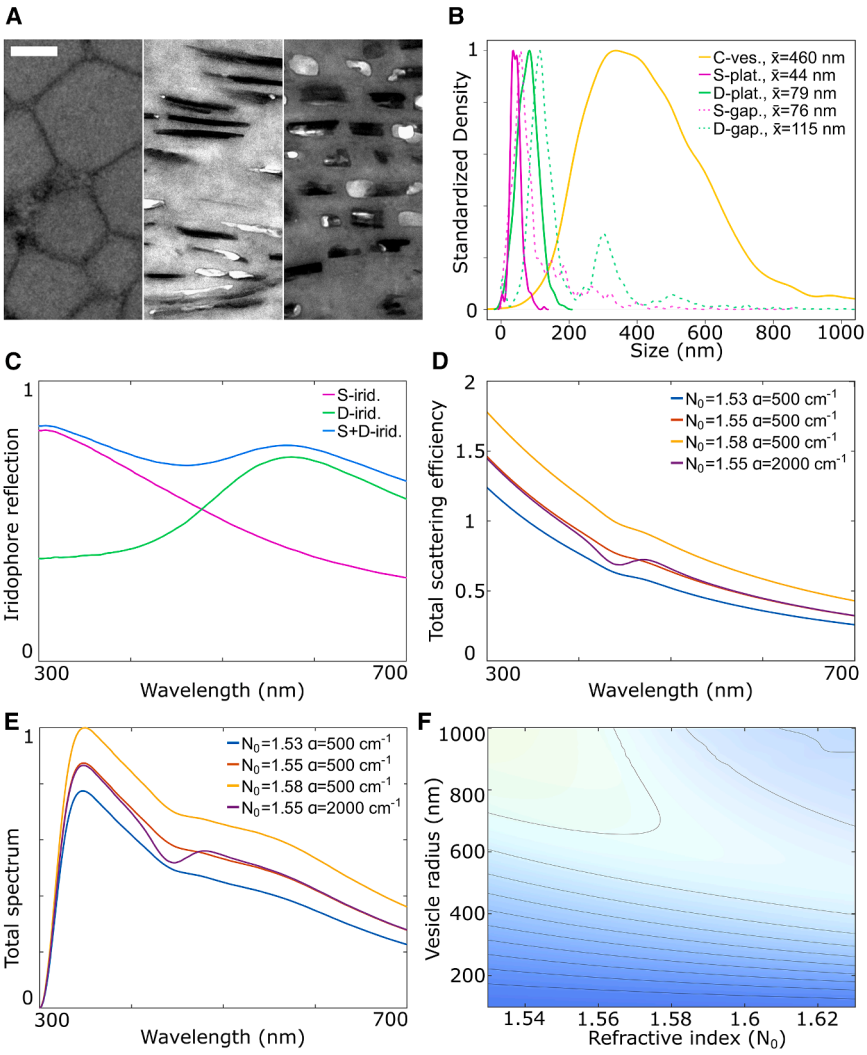

Figure 8. Models of UV-blue color production suggest close interplay of reflectance on iridophores and scattering by carotenoid vesicles

(A) Detailed view of the CPEs. From left to right, carotenoid vesicles inside epidermal xanthophore-like cells, reflecting platelets of S-iridophores, reflecting platelets of D-iridophores. *P. muralis*. Scale bars, 250 nm.

(B) Sizes of CPEs measured from TEM images in *P. muralis*. The diameter of carotenoid vesicles of epidermal xanthophore-like cells (yellow solid line, average 460 nm, SD = 241 nm, N = 4,929), the thickness of reflecting platelets of S-iridophores (magenta solid line, average 44 nm, SD = 17 nm, N = 411), the thickness of reflecting platelets of D-iridophores (green solid line, average 79 nm, SD = 31 nm, N = 607), the gap between reflecting platelets of S-iridophores (magenta dashed line, average 76 nm, SD = 76 nm, N = 97), the gap between reflecting platelets of D-iridophores (green dashed line, average 115 nm, SD = 115, N = 145).

(C) Theoretical prediction of reflectance for individual types of iridophores (magenta for S-iridophores and green for D-iridophores) and the prediction of their interaction when equally represented (blue).

(D) Estimated wavelength-dependent forward scattering efficiency of carotenoid vesicles of xanthophore-like cells with various parameterizations. Note the absorption band around 450 nm especially prominent when N_0 = 1.55 and α = 2,000 cm^{-1}.

(E) Overall scattered light from the UV-blue skin patch as a result of the interaction among the three types of CPEs. N_0 is the intrinsic refractive index and α is the peak absorption coefficient at 450 nm (particular values are shown in the legend inside the graphs).

(F) RGB simulation based on predicted spectra when the size r_0 and refractive index of xanthophore-like carotenoid vesicles change. Note that in some combinations of carotenoid concentrations (which are related to refractive index) and carotenoid vesicle sizes, the resulting color is rather yellow-green-white while for others it is clearly blue. Peak absorption coefficient was considered α = 500 cm^{-1}. See also Figures S7–S9.

interaction between two morphologically distinct iridophore classes (S-iridophores and D-iridophores) and a population of epidermal xanthophore-like cells. This intricate arrangement highlights the central role played by iridophores in short-wavelength color production. However, our findings reveal that the UV-blue coloration is not generated by iridophore reflection alone, but its production also involves light scattering by spherical, yellow carotenoid-containing vesicles within the epidermal xanthophore-like cells. The interplay between the reflecting iridophores and pigment containing cells seems to be essential for the striking UV-blue coloration observed in the ventrolateral skin of these lizards.

This arrangement, with xanthophore-like cells in the epidermis underlain by S- and D-iridophores and melanophores in the dermis deviates from the standard arrangement of chromatophores typically found in color patches of lizards. In contrast, the basic organization of pigment cells in the rest of the body agrees with the dermal chromatophore unit concept,[9] i.e., stacked pigment cells within the dermis, with xanthophores at the top just below the basal lamina, and iridophores and melanophores lying beneath them.[7] The composition of colored skin outside of the ventrolateral region remains largely conserved across species and body regions, even though the three *Podarcis* species show various colors on their ventral and dorsal surfaces, ranging from white and brown to yellow-orange, but also showing green to blue hues. Thus, the composition of the UV-blue ventrolateral patches sets them apart from the rest of the body, even though the sequence of pigment cell types from the body surface inward remains essentially similar. Comparison across three species of the genus *Podarcis* shows that the arrangement of the UV-blue patches is consistent across different species (Figure 4). The interspecific similarity of the reflectance spectra for this region further supports the idea that the cellular arrangement is associated with its distinctive UV-blue coloration. The cellular organization of the UV-blue

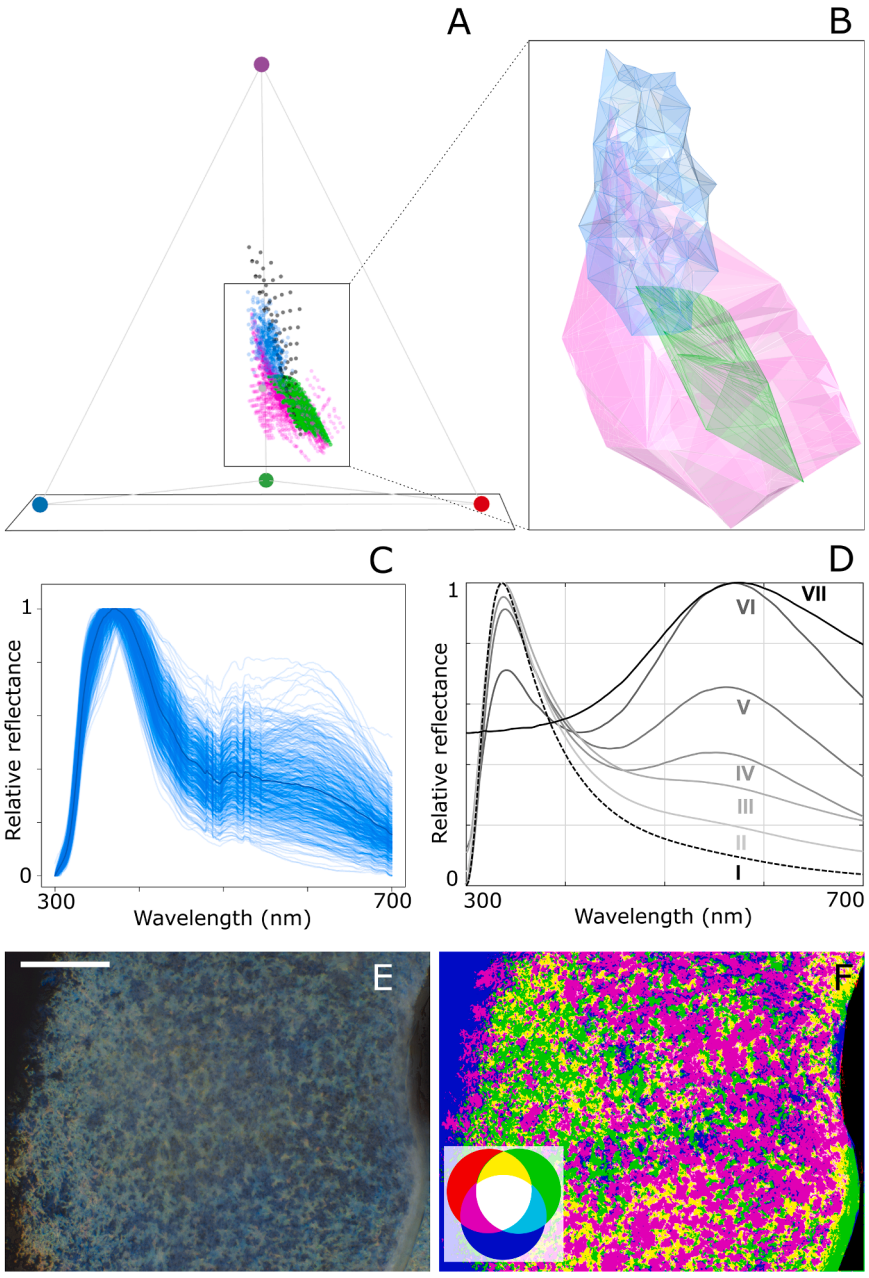

Figure 9. Evaluating model fit to measured UV-blue patch reflectance and its intraspecific variation

(A) Tetrahedral color-space showing variation in real measured spectra of UV-blue patches (blue, *N* = 541), the traditional understanding of color production based on xanthophores as absorbing "filter" (green, *N* = 2,305), and the predicted spectra of the model that considers xanthophores as "scatterers" (magenta, *N* = 2,305). Black points represent the effect of a cellular "mosaic" of the color patch (*N* = 132, compare measured intraspecific variation of UV-blue patches of *P. muralis* in (A) and predicted spectra in D).

(B) Volume overlap between real spectra of UV-blue patches (blue), scattering mechanism predicted spectra (magenta), and filter mechanism predicted spectra (green). The scattering mechanism shows vast overlap with real data, while the filter mechanism shows only poor overlap with measured data.

(C) Measured reflectance spectra of UV-blue patches of *P. muralis*.

(D) The effect of cellular "mosaic" composition of the scale: I—100% cover by S-iridophores, 100% cover by epidermal xanthophore-like cells, and 0% D-iridophores; II—90% cover by S-iridophores, 90% cover by epidermal xanthophore-like cells, and 10% D-iridophores; III—70% cover by S-iridophores, 70% cover by epidermal xanthophore-like cells, and 30% D-iridophores; IV—50% cover by S-iridophores, 50% cover by epidermal xanthophore-like cells, and 50% D-iridophores; V—30% cover by S-iridophores, 30% cover by epidermal xanthophore-like cells, and 70% D-iridophores; VI—10% cover by S-iridophores, 10% cover by epidermal xanthophore-like cells, and 90% D-iridophores; VII—0% cover by S-iridophores, 0% cover by epidermal xanthophore-like cells, and 100% D-iridophores.

(E) Representative image from a stereomicroscope illustrating the concept of mosaic organization within the UV-blue patch.

(F) Composite image illustrating the mosaic nature of the UV-blue patch, constructed from three channels: a blue channel (grayscale-thresholded image of dark pixels representing the melanophore background), a green channel (grayscale-thresholded image of light pixels representing the D-iridophore background), and a red channel (color-thresholded image of pixels within a defined range of blue values representing the combined effect of xanthophore-like cells and S-iridophores), see further details in Figure S8. Circles in the lower left corner illustrate how the three channels combine. The red channel overlaps locally either with the blue channel (magenta) or with the green channel (yellow), whereas overlap between the blue and green channels is almost never observed. Changes in the relative coverage of different pigment cell types are therefore expected to primarily alter the relative proportions of green, yellow, and magenta regions. It is important to note that this schematic is purely illustrative. Scale bars same for (E and F), 200 μm. See also Figure S10.

color patches (Figure 3) is, to the best of our knowledge, the most complex color-producing system in *Podarcis* lizards, and it is also very different from the color-producing mechanisms reported in other vertebrates.[7]

Our results indicate a dual contribution of pigment cells within the UV-blue ventrolateral patches to coloration: S-iridophores, together with xanthophore-like cells, generate the short-wavelength main peak, whereas D-iridophores reflect longer wavelengths, producing the secondary peak observed in the spectrum (Figure 8). Multiple layers of iridophores are relatively common in amphibians and reptiles,[7,21] but what is unusual in *Podarcis* is that these layers consist of two distinct classes of iridophores differing in platelet morphology. Dual classes of iridophores were first described in *Danio rerio*, where they generate iridescence.[40] This organization later received particular attention in chameleons, in which pronounced differences in crystal

dimensions underlie color change and thermal regulation[13] and has also been reported in the gecko *Pachydactylus rangei*, where it contributes to fluorescence.[41] Dual iridophore layers were framed as an evolutionary innovation exclusive to chameleons, a conclusion supported by the presence of unusually large differences in crystal thickness in that system. In those cases, platelet dimensions remain distinguishable even when inferred indirectly from crystal-loss voids, a common approach in ultrastructural studies of iridophores. Our observation of two distinct iridophore classes in *Podarcis* suggests that similar organization may occur more broadly across taxa. However, when reflecting platelets are extremely thin, such as those of Japanese fire-bellied newt,[42] indirect inference from void size lacks sufficient sensitivity to resolve small but optically meaningful differences, increasing the likelihood that such organization has been overlooked in other taxa.

The different morphology of platelets in the two iridophore layers implies distinct optical properties that must be explicitly incorporated into models of color production. Earlier modeling approaches derived expected reflectance wavelengths of iridophores from crystal-size distributions using simple thin-film interference equations,[6,43,44] but these are insufficient when multiple iridophore layers are present as they do not account for multiple reflections between them. More recent models,[5,21,45] including ours, account for these interactions and are therefore better suited to systems with two iridophore classes.

A widely accepted paradigm holds that combining a blue, iridophore-based structural color with yellow, xanthophore-based pigmentation should yield a green coloration.[12,46–48] In line with this view, blue skin has usually been associated with either a low density of xanthophores or reduced pigment content (axanthism): dermal xanthophores have been reported in blue regions,[49] but sometimes in small numbers,[50] or with few vesicles,[6] or with mostly transparent pterins.[44] Thus, blue coloration has typically been attributed to reduced xanthophore density or pigment content, preventing the usual shift toward longer wavelengths.

In *Podarcis*, however, this explanation does not apply. Despite abundant yellow carotenoid-containing epidermal xanthophore-like cells above S-iridophores predicted to reflect UV-blue light, the ventrolateral patches do not shift toward green. We therefore suggest that these xanthophore-like cells do not act solely as absorptive filters; instead, their carotenoid vesicles function as scatterers that enhance short-wavelength reflectance from S-iridophores, producing the observed UV-blue coloration. Our results show that vesicles of xanthophore-like cells alone cannot generate UV-blue coloration by backscattering incident light, but they can still contribute to color production by forward-scattering UV-blue light (Figure 8D) reflected by S-iridophores (Figure 8C), thereby amplifying the short-wavelength signal. This is consistent with the fact that absorption by yellow carotenoids not only attenuates reflectance around 450 nm but is coupled to wavelength-dependent changes in refractive index, which can promote additional short-wavelength scattering by carotenoid vesicles.[51] As a result, the combined action of S-iridophores and carotenoid vesicles produces reflectance spectra that cannot be reproduced by traditional models treating xanthophores as simple absorptive filters (Figure 9), and instead points to a key role of vesicle morphology.

While Mie scattering is a general optical principle, its impact here depends on vesicle size and pigment concentration within the vesicles (Figure 8F). For scattering to produce distinct colors, CPE sizes must be relatively uniform, whereas greater variability in size leads to spectral broadening, diminishing the effect. Additionally, scattering efficiency is influenced by pigment saturation and refractive index. Thus, in other skin regions of *Podarcis*, where dermal xanthophores contain a mix of pigments and show greater size variation (Figure 2E; see also Andrade et al.[35]), their contribution to scattering may be negligible. Instead, xanthophores in these areas likely act only as a filtering layer. Consistent with this interpretation, our visual modeling suggests that the scatterer model is not incompatible with the filter model; rather, their predicted color spaces overlap significantly (Figure 9B). This may be because, in spectral regions where the filter mechanism dominates, the contribution of Mie scattering is weak, making the xanthophores function primarily as absorptive layers. Overall, our results suggest that the contribution of xanthophore vesicles to coloration is context dependent. In some regions, they may act as scatterers, while in others, they function primarily as absorptive filters.

Within the UV-blue patches, the blue and UV coloration appears relatively uniform across the patch surface when viewed at low magnification (Figures 1G and 1H). This suggests a broadly regular distribution of epidermal xanthophore-like cells together with underlying S-iridophores (see also Figure S1). However, closer inspection of individual scales (Figures 9E and 9F) reveals that the cellular composition forms an irregular mosaic across the patch surface, and the observed colors likely represent a local collective effect of this fine-scale heterogeneity. Notably, the greenish micro-regions are brighter than the surrounding blue micro-regions of the scale, which is consistent with a local contribution of deeper D-iridophores beneath the S-iridophore layer. We therefore interpret the mosaic pattern as arising from a heterogeneous distribution of background melanophores and D-iridophores underlying the more uniformly distributed S-iridophores and epidermal xanthophore-like cells. This mosaic organization leads to spatially variable contributions of the different pigment cell types and may explain the pronounced inter-individual variation in the secondary reflectance peak observed in *P. muralis* (Figures 9C and 9D). Such non-uniform distributions of pigment cells are consistent with expectations for systems shaped by self-organizing processes, which operate on within scale patterning until stable organization is reached.[52] Because UV-blue patches develop only postnatally,[53] early postnatal development likely represents the key window in which the cellular composition of these patches is established. However, it is also possible that the UV-blue patches keep changing in adulthood in a condition-dependent manner, as is the case with many signals of quality.[54]

The presence of xanthophore-like cells in the epidermis is striking, as chromatophores containing carotenoids or pterins are typically confined to the dermis in ectothermic vertebrates.[10] Epidermal xanthophores have been reported only in a few fishes and caudate amphibians,[55–60] often in the context of

developmental migrations during metamorphosis. Despite extensive work on dermal pigment cells,[61–63] the biology of epidermal pigment cells remains virtually unexplored. Their occurrence in *Podarcis* is therefore notable and may influence color production, given differences in refractive index between epidermis and dermis[64,65] and altered spatial relationships to the underlying iridophores. This raises the possibility that epidermal positioning itself contributes to the optical properties of these patches.

Ultraviolet reflectance plays a crucial role in animal communication, influencing mate choice, species recognition, and social interactions across a wide range of taxa.[1] Many lizards, including *Podarcis*, use UV-reflective patches as visual signals, yet the mechanisms generating these signals have remained poorly understood. Although structural coloration in lizards is usually attributed to iridophores, previous studies have rarely addressed how UV reflectance specifically arises in skin patches.[7] Our study provides mechanistic explanation for UV reflectance in lizard skin, showing that its production involves a more elaborate combination of cellular components than previously assumed. UV patches are known to influence social interactions in lacertid lizards,[29,66–69] highlighting that the interplay between cellular organization and signaling function may be an underappreciated aspect of reptile coloration. By clarifying the origin of UV reflectance, our findings reveal integrated pigmentary and structural contributions and open the way to a deeper understanding of how UV coloration functions as a signal.

Our study reveals a previously undescribed mechanism of UV-blue color production in *Podarcis* lizards, in which two distinct classes of iridophores interact with epidermal xanthophore-like cells to generate short-wavelength reflectance. Departing from the canonical dermal chromatophore arrangement, this system shows that epidermal xanthophores can enhance UV-blue coloration through scattering rather than filtering alone, highlighting a more integrated structural-pigmentary relation than previously recognized.

Although the scattering contribution of pigment-filled vesicles is especially evident in *Podarcis*, the underlying physical principle is general: absorbing pigments alter local refractive indices and therefore inevitably contribute to light scattering, an effect that is further enhanced when pigments are stored in spherical vesicles. Many vertebrate integuments, from skin to feathers, contain such pigment inclusions whose scattering roles remain poorly characterized. Identifying cases where scattering pigments interact with structural reflectors may reveal additional, currently overlooked mechanisms of color production.

A key next step will be developing experimental approaches that separate pigmentary and structural contributions without altering native optical properties of the CPEs. Mechanical manipulations, pH shifts, enzymatic reactions, or cell isolation all may change optical properties. This is why methods to test experimentally predictions of models, such as ours, remain challenging.

It remains unclear whether epidermal xanthophore-like cells are homologous to dermal xanthophores and how S- and D-iridophores are developmentally related. Although the two iridophore classes differ morphologically, the regulation of reflecting platelet formation remains largely unresolved, as under the experimental conditions applied here, Raman spectroscopy did not reveal detectable differences in platelet composition.

At a broader scale, this work invites an evolutionary perspective on how and why this system evolved. UV reflecting ventrolateral patches are widespread in lacertids and related species exhibit UV-yellow or UV-green patches in the same region. Determining whether the cellular arrangement described here is shared across the family, and how such variation maps onto functional roles, is a promising direction for comparative research. More generally, the discovery of this intricate and previously overlooked skin architecture in a well-studied group highlights how incomplete our understanding of vertebrate coloration remains and underscores the need to investigate similar mechanisms in other taxa.

Limitations of the study

This study has several limitations that should be considered when interpreting the results. First, we did not include basal lamina, and lineage- or cell-type-specific markers to conclusively identify the epidermal carotenoid-bearing cells as xanthophores. Their epidermal localization and chromatophore identity are therefore inferred primarily from morphological criteria. While these observations are consistent with our interpretation, independent molecular validation would further strengthen the assignment, particularly given that chromatophores are most commonly described as dermal structures.

Second, although the spatial distribution of carotenoid vesicles, spectroscopic mapping, and optical modeling collectively support a scattering contribution to UV-blue reflectance, we did not perform direct perturbation experiments (e.g., carotenoid depletion, epidermal manipulation, or optical index matching) to test necessity or sufficiency. Thus, the proposed mechanism is supported by convergent morphological, spectroscopic, and modeling evidence but remains to be validated through causal experimental approaches.

Finally, certain optical parameters were not measured directly but were instead estimated based on values reported in the literature and constrained within biologically plausible ranges. Although this approach is standard in optical modeling, direct empirical characterization of these parameters could allow a quantitative refinement in future work.

RESOURCE AVAILABILITY

Lead contact

Further information and requests may be directed to the lead contact, Dr. Jindřich Brejcha (brejcha@natur.cuni.cz).

Materials availability

This study did not generate new unique reagents.

Data and code availability

- Original data are available at https://doi.org/10.17632/d95wywzjd7.2.[32]
- Original code is available at https://doi.org/10.17632/d95wywzjd7.2.[32]
- Any additional information required to reanalyze the data reported in this paper is available from the lead contact upon request.

ACKNOWLEDGMENTS

We would like to thank the Verdugo Lab, especially Patricia García Tárraga and Susana González, for their support, Mario Soriano for assistance with TEM sample preparation, and Anna Kawamoto for assistance with sampling. We also thank Alicia Bartolomé for dedicated animal care. We are also grateful to Joaquín Baixeras for help with macroscopic imaging, and to Roman Rozínek

for providing a lizard from Natura Servis breeding facility to pilot non-invasive Raman experiments. Special thanks go to Javier Ábalos for his help with sampling, photodocumentation, sample preparation, and for many insightful discussions on the topic. Collaboration between JB and TO has been supported by FCT grant 2022.03774.PTDC. This study was supported in part by grant PID2019-104721GB-I00 of the Spanish Ministerio de Ciencia e Innovación and grant AICO/2021/113 from the Conselleria d'Innovació, Universitats, Ciència i Societat Digital to E.F. and G.P.L. Computational resources were provided by the e-INFRA CZ project (ID: 90254), supported by the Ministry of Education, Youth and Sports of the Czech Republic. This study is dedicated to the memory of José Manuel García Verdugo.

AUTHOR CONTRIBUTIONS

Conceptualization, J.B. and E.F.; methodology, J.B., T.O., P. Mojzeš, P. Maršík, J.P., and E.F.; investigation, J.B., T.O., G.P.L., P. Mojzeš, P. Maršík, J.P., T.V., and E.F.; writing – original draft, J.B., T.O., and E.F.; writing – review and editing, J.B., T.O., G.P.L., P. Mojzeš, P. Maršík, and E.F.; funding acquisition, J.B.,T.O., G.P.L., and E.F.; resources, E. F., supervision, J.B. and E.F.

DECLARATION OF INTERESTS

The authors declare no competing interests.

DECLARATION OF GENERATIVE AI AND AI-ASSISTED TECHNOLOGIES IN THE WRITING PROCESS

The first draft of this work was written without the use of an AI, even though Google Translate is a tool commonly used by J.B. During editing process, J.B. used mostly ChatGPT to translate certain expressions from Czech, which is J.B.'s native language, to English. J.B. also used ChatGPT to incorporate some notes and ideas into sentences during the editing process. After using this tool, the authors reviewed and edited the content multiple times and take full responsibility for the content of the publication.

STAR★METHODS

Detailed methods are provided in the online version of this paper and include the following:

- KEY RESOURCES TABLE
- EXPERIMENTAL MODEL AND STUDY PARTICIPANT
  - Animal handling and treatment
- METHOD DETAILS
  - Color measurements and photography
  - Light microscopy
  - Electron microscopy
  - Pigment analyses
  - Modeling of color production
  - Visual modeling
- QUANTIFICATION AND STATISTICAL ANALYSIS
  - Quantification of subcellular structures
  - Statistical comparison of S- and D-iridophore platelets
  - Optical modeling and spectral simulations
  - Visual modeling and comparison with empirical spectra
  - Sample size determination, randomization, and exclusion criteria
  - Definition of central tendency and significance

SUPPLEMENTAL INFORMATION

Supplemental information can be found online at https://doi.org/10.1016/j.isci.2026.116106.

Received: August 1, 2025
Revised: December 22, 2025
Accepted: April 2, 2026

REFERENCES

1. Cuthill, I.C., Allen, W.L., Arbuckle, K., Caspers, B., Chaplin, G., Hauber, M.E., Hill, G.E., Jablonski, N.G., Jiggins, C.D., Kelber, A., et al. (2017). The biology of color. Science *357*, eaan0221. https://doi.org/10.1126/science.aan0221.
2. Wiens, J.J., and Emberts, Z. (2025). How life became colourful: colour vision, aposematism, sexual selection, flowers, and fruits. Biol. Rev. *100*, 308–326. https://doi.org/10.1111/brv.13141.
3. Shawkey, M.D., and D'Alba, L. (2017). Interactions between colour-producing mechanisms and their effects on the integumentary colour palette. Philos. Trans. R. Soc. Lond. B Biol. Sci. *372*, 20160536. https://doi.org/10.1098/rstb.2016.0536.
4. Olsson, M., Stuart-Fox, D., and Ballen, C. (2013). Genetics and evolution of colour patterns in reptiles. Semin. Cell Dev. Biol. *24*, 529–541. https://doi.org/10.1016/j.semcdb.2013.04.001.
5. Saenko, S.V., Teyssier, J., Van Der Marel, D., and Milinkovitch, M.C. (2013). Precise colocalization of interacting structural and pigmentary elements generates extensive color pattern variation in Phelsumalizards. BMC Biol. *11*, 105. https://doi.org/10.1186/1741-7007-11-105.
6. Haisten, D.C., Paranjpe, D., Loveridge, S., and Sinervo, B. (2015). The Cellular Basis of Polymorphic Coloration in Common Side-Blotched Lizards, *Uta stansburiana*. Herpetologica *71*, 125–135. https://doi.org/10.1655/HERPETOLOGICA-D-13-00091.
7. Kuriyama, T., Murakami, A., Brandley, M., and Hasegawa, M. (2020). Blue, Black, and Stripes: Evolution and Development of Color Production and Pattern Formation in Lizards and Snakes. Front. Ecol. Evol. *8*, 232. https://doi.org/10.3389/fevo.2020.00232.
8. Shawkey, M.D., Morehouse, N.I., and Vukusic, P. (2009). A protean palette: colour materials and mixing in birds and butterflies. J. R. Soc. Interface *6*, S221–S231. https://doi.org/10.1098/rsif.2008.0459.focus.
9. Bagnara, J.T., Taylor, J.D., and Hadley, M.E. (1968). The Dermal Chromatophore Unit. J. Cell Biol. *38*, 67–79. https://doi.org/10.1083/jcb.38.1.67.
10. Schartl, M., Larue, L., Goda, M., Bosenberg, M.W., Hashimoto, H., and Kelsh, R.N. (2016). What is a vertebrate pigment cell? Pigment Cell Melanoma Res. *29*, 8–14. https://doi.org/10.1111/pcmr.12409.
11. Bagnara, J.T., Matsumoto, J., Ferris, W., Frost, S.K., Turner, W.A., Tchen, T.T., and Taylor, J.D. (1979). Common Origin of Pigment Cells. Science *203*, 410–415. https://doi.org/10.1126/science.760198.
12. Bagnara, J.T., Fernandez, P.J., and Fujii, R. (2007). On the blue coloration of vertebrates. Pigment. Cell Res. *20*, 14–26. https://doi.org/10.1111/j.1600-0749.2006.00360.x.
13. Teyssier, J., Saenko, S.V., Van Der Marel, D., and Milinkovitch, M.C. (2015). Photonic crystals cause active colour change in chameleons. Nat. Commun. *6*, 6368. https://doi.org/10.1038/ncomms7368.
14. Brebner, J.S., Loconsole, M., Hanley, D., and Vasas, V. (2024). Through an animal's eye: the implications of diverse sensory systems in scientific experimentation. Proc. Biol. Sci. *291*, 20240022. https://doi.org/10.1098/rspb.2024.0022.
15. Eaton, M.D., and Lanyon, S.M. (2003). The ubiquity of avian ultraviolet plumage reflectance. Proc. Biol. Sci. *270*, 1721–1726. https://doi.org/10.1098/rspb.2003.2431.
16. Crowell, H.L., Curlis, J.D., Weller, H.I., and Davis Rabosky, A.R. (2024). Ecological drivers of ultraviolet colour evolution in snakes. Nat. Commun. *15*, 5213. https://doi.org/10.1038/s41467-024-49506-4.
17. Baden, T., and Osorio, D. (2019). The Retinal Basis of Vertebrate Color Vision. Annu. Rev. Vis. Sci. *5*, 177–200. https://doi.org/10.1146/annurev-vision-091718-014926.
18. Goda, M., and Fujii, R. (1995). Blue Chromatophores in Two Species of Callionymid Fish. Zoolog. Sci. *12*, 811–813. https://doi.org/10.2108/zsj.12.811.

19. San-Jose, L.M., Granado-Lorencio, F., Sinervo, B., and Fitze, P.S. (2013). Iridophores and Not Carotenoids Account for Chromatic Variation of Carotenoid-Based Coloration in Common Lizards (*Lacerta vivipara*). Am. Nat. *181*, 396–409. https://doi.org/10.1086/669159.

20. Brejcha, J., Bataller, J.V., Bosáková, Z., Geryk, J., Havlíková, M., Kleisner, K., Maršík, P., and Font, E. (2019). Body coloration and mechanisms of colour production in Archelosauria: the case of deirocheline turtles. R. Soc. Open Sci. *6*, 190319. https://doi.org/10.1098/rsos.190319.

21. Twomey, E., Kain, M., Claeys, M., Summers, K., Castroviejo-Fisher, S., and Van Bocxlaer, I. (2020). Mechanisms for Color Convergence in a Mimetic Radiation of Poison Frogs. Am. Nat. *195*, E132–E149. https://doi.org/10.1086/708157.

22. Hecht, E. (2001). Optics, 4th ed. (Addison-Wesley).

23. Prum, R.O., Torres, R.H., Williamson, S., and Dyck, J. (1998). Coherent light scattering by blue feather barbs. Nature *396*, 28–29. https://doi.org/10.1038/23838.

24. Sun, J., Bhushan, B., and Tong, J. (2013). Structural coloration in nature. RSC Adv. *3*, 14862. https://doi.org/10.1039/c3ra41096j.

25. Shang, G., Maiwald, L., Renner, H., Jalas, D., Dosta, M., Heinrich, S., Petrov, A., and Eich, M. (2018). Photonic glass for high contrast structural color. Sci. Rep. *8*, 7804. https://doi.org/10.1038/s41598-018-26119-8.

26. Schertel, L., Siedentop, L., Meijer, J., Keim, P., Aegerter, C.M., Aubry, G.J., and Maret, G. (2019). The Structural Colors of Photonic Glasses. Adv. Opt. Mater. *7*, 1900442. https://doi.org/10.1002/adom.201900442.

27. Sinnott-Armstrong, M.A., Ogawa, Y., Van De Kerkhof, G.T., Vignolini, S., and Smith, S.D. (2022). Convergent evolution of disordered lipidic structural colour in the fruits of *Lantana strigocamara* (syn. *L. camara* hybrid cultivar). New Phytol. *235*, 898–906. https://doi.org/10.1111/nph.18262.

28. Henze, M.J., Lind, O., Wilts, B.D., and Kelber, A. (2019). Pterin-pigmented nanospheres create the colours of the polymorphic damselfly *Ischnura elegans*. J. R. Soc. Interface *16*, 20180785. https://doi.org/10.1098/rsif.2018.0785.

29. Font, E., Pérez I De Lanuza, G., and Sampedro, C. (2009). Ultraviolet reflectance and cryptic sexual dichromatism in the ocellated lizard, *Lacerta* (*Timon*) *lepida* (Squamata: Lacertidae). Biol. J. Linn. Soc. *97*, 766–780. https://doi.org/10.1111/j.1095-8312.2009.01251.x.

30. Font, E., and Molina-Borja, M. (2004). Ultraviolet reflectance of color patches in Gallotia galloti from Tenerife, Canary Islands. In Biol. Lacertid Lizards Evol. Ecol. Perspect. Inst. Menorquí D'Estudis, pp. 201–221.

31. Pérez i De Lanuza, G., and Font, E. (2015). Differences in conspicuousness between alternative color morphs in a polychromatic lizard. Behav. Ecol. *26*, 1432–1446. https://doi.org/10.1093/beheco/arv075.

32. Brejcha, J., Ostatnický, T., Lanuza, G., Mojzeš, P., Maršík, P., Pilátová, J., Vargicova, T., and Font, E. (2025). Dataset : A study of Unravelling the structural and pigmentary mechanisms of UV color signal production in *Podarcis* wall lizards Brejcha et al. Mendeley Data V2. https://doi.org/10.17632/d95wywzjd7.2.

33. Gillbro, T., and Cogdell, R.J. (1989). Carotenoid fluorescence. Chem. Phys. Lett. *158*, 312–316. https://doi.org/10.1016/0009-2614(89)87342-7.

34. Kleinegris, D.M.M., Van Es, M.A., Janssen, M., Brandenburg, W.A., and Wijffels, R.H. (2010). Carotenoid fluorescence in *Dunaliella salina*. J. Appl. Phycol. *22*, 645–649. https://doi.org/10.1007/s10811-010-9505-y.

35. Andrade, P., Pinho, C., Pérez I De Lanuza, G., Afonso, S., Brejcha, J., Rubin, C.-J., Wallerman, O., Pereira, P., Sabatino, S.J., Bellati, A., et al. (2019). Regulatory changes in pterin and carotenoid genes underlie balanced color polymorphisms in the wall lizard. Proc. Natl. Acad. Sci. USA *116*, 5633–5642. https://doi.org/10.1073/pnas.1820320116.

36. Bohren, C.F., and Huffman, D.R. (2008). Absorption and Scattering of Light by Small Particles (John Wiley & Sons).

37. Bendit, E.G., and Ross, D. (1961). A Technique for Obtaining the Ultraviolet Absorption Spectrum of Solid Keratin. Appl. Spectrosc. *15*, 103–105. https://doi.org/10.1366/000370261774426957.

38. Yunus, W.M., and Rahman, A.B. (1988). Refractive index of solutions at high concentrations. Appl. Opt. *27*, 3341–3343. https://doi.org/10.1364/AO.27.003341.

39. Tan, C.-Y., and Huang, Y.-X. (2015). Dependence of Refractive Index on Concentration and Temperature in Electrolyte Solution, Polar Solution, Nonpolar Solution, and Protein Solution. J. Chem. Eng. Data *60*, 2827–2833. https://doi.org/10.1021/acs.jced.5b00018.

40. Frohnhöfer, H.G., Krauss, J., Maischein, H.-M., and Nüsslein-Volhard, C. (2013). Iridophores and their interactions with other chromatophores are required for stripe formation in zebrafish. Development *140*, 2997–3007. https://doi.org/10.1242/dev.096719.

41. Prötzel, D., Heß, M., Schwager, M., Glaw, F., and Scherz, M.D. (2021). Neon-green fluorescence in the desert gecko *Pachydactylus rangei* caused by iridophores. Sci. Rep. *11*, 297. https://doi.org/10.1038/s41598-020-79706-z.

42. Kuriyama, T., Koike-Minemoto, K., Morimoto, G., and Miyaji, K. (2026). Pigment cell mechanism of bluish-purple nuptial colouration in the Japanese fire-bellied newt *Cynops pyrrhogaster*. J. Zool. jzo.70107. https://doi.org/10.1111/jzo.70107.

43. Fujii, R. (1993). Cytophysiology of Fish Chromatophores. In International Review of Cytology, K.W. Jeon, M. Friedlander, and J. Jarvik, eds. (Elsevier), pp. 191–255. https://doi.org/10.1016/S0074-7696(08)61876-8.

44. Morrison, R.L., Rand, M.S., and Frost-Mason, S.K. (1995). Cellular Basis of Color Differences in Three Morphs of the Lizard *Sceloporus undulatus erythrocheilus*. Copeia *1995*, 397–408. https://doi.org/10.2307/1446903.

45. Maia, R., Caetano, J.V.O., Báo, S.N., and Macedo, R.H. (2009). Iridescent structural colour production in male blue-black grassquit feather barbules: the role of keratin and melanin. J. R. Soc. Interface *6*, S203–S211. https://doi.org/10.1098/rsif.2008.0460.focus.

46. Finger, E. (1995). Visible and UV coloration in birds: Mie scattering as the basis of color in many bird feathers. Naturwissenschaften *82*, 570–573. https://doi.org/10.1007/BF01140249.

47. Macedonia, J.M., James, S., Wittle, L.W., and Clark, D.L. (2000). Skin Pigments and Coloration in the Jamaican Radiation of Anolis Lizards. J. Herpetol. *34*, 99–109. https://doi.org/10.2307/1565245.

48. Grether, G.F., Kolluru, G.R., and Nersissian, K. (2004). Individual colour patches as multicomponent signals. Biol. Rev. *79*, 583–610. https://doi.org/10.1017/S1464793103006390.

49. Goda, M., and Kuriyama, T. (2021). Physiological and Morphological Color Changes in Teleosts and in Reptiles. In Pigments, Pigment Cells and Pigment Patterns, H. Hashimoto, M. Goda, R. Futahashi, R. Kelsh, and T. Akiyama, eds. (Springer Singapore), pp. 387–423. https://doi.org/10.1007/978-981-16-1490-3_13.

50. Szydłowski, P., Madej, J.P., and Mazurkiewicz-Kania, M. (2017). Histology and ultrastructure of the integumental chromatophores in tokay gecko (*Gekko gecko*) (Linnaeus, 1758) skin. Zoomorphology *136*, 233–240. https://doi.org/10.1007/s00435-017-0348-9.

51. Sai, T., Froufe-Pérez, L.S., Scheffold, F., Wilts, B.D., and Dufresne, E.R. (2023). Structural color from pigment-loaded nanostructures. Soft Matter *19*, 7717–7723. https://doi.org/10.1039/D3SM00961K.

52. Manukyan, L., Montandon, S.A., Fofonjka, A., Smirnov, S., and Milinkovitch, M.C. (2017). A living mesoscopic cellular automaton made of skin scales. Nature *544*, 173–179. https://doi.org/10.1038/nature22031.

53. Abalos, J., Bartolomé, A., De Lanuza, G.P.I., Aubret, F., and Font, E. (2026). Cryptic Ontogenetic Changes in the Ventral Coloration of a Color Polymorphic Wall Lizard (*Podarcis muralis*). J. Exp. Zool. Part Ecol. Integr. Physiol. *345*, 39–57. https://doi.org/10.1002/jez.70035.

54. Bradbury, J.W., and Vehrencamp, S.L. (2011). Principles of Animal Communication (Sinauer Associates).

55. Hirata, M., Nakamura, K.i., Kanemaru, T., Shibata, Y., and Kondo, S. (2003). Pigment cell organization in the hypodermis of zebrafish. Dev. Dyn. *227*, 497–503. https://doi.org/10.1002/dvdy.10334.

56. Obika, M., and Meyer-Rochow, V.B. (1990). Dermal and Epidermal Chromatophores of the Antarctic Teleost *Trematomus bernacchii*. Pigment. Cell Res. *3*, 33–37. https://doi.org/10.1111/j.1600-0749.1990.tb00259.x.

57. Ferrer, C., Solano, F., and Zuasti, A. (1999). Ultrastructural and biochemical analysis of epidermal xanthophores and dermal chromatophores of the teleost *Sparus aurata*. Histol. Histopathol. *14*, 383–390. https://doi.org/10.14670/HH-14.383.

58. Forbes, M.S., Zaccaria, R.A., and Dent, J.N. (1973). Developmental cytology of chromatophores in the red-spotted newt. Am. J. Anat. *138*, 37–71. https://doi.org/10.1002/aja.1001380104.

59. Oliphant, L.W. (1973). Epidermal xanthophores in a salamander. Can. J. Zool. *51*, 1007–1009. https://doi.org/10.1139/z73-146.

60. Burgon, J.D. (2018). Evolutionary and Genomic Associations of Colour and Pattern in Fire and Alpine Salamanders (*Salamandra Spp.*) (University of Glasgow).

61. Irion, U., Singh, A.P., and Nüsslein-Volhard, C. (2016). The Developmental Genetics of Vertebrate Color Pattern Formation. Curr. Top. Dev. Biol. *117*, 141–169. https://doi.org/10.1016/bs.ctdb.2015.12.012.

62. Kondo, S., Watanabe, M., and Miyazawa, S. (2021). Studies of Turing pattern formation in zebrafish skin. Philos. Trans. A Math. Phys. Eng. Sci. *379*, 20200274. https://doi.org/10.1098/rsta.2020.0274.

63. Parichy, D.M. (2021). Evolution of pigment cells and patterns: recent insights from teleost fishes. Curr. Opin. Genet. Dev. *69*, 88–96. https://doi.org/10.1016/j.gde.2021.02.006.

64. Ding, H., Lu, J.Q., Wooden, W.A., Kragel, P.J., and Hu, X.-H. (2006). Refractive indices of human skin tissues at eight wavelengths and estimated dispersion relations between 300 and 1600 nm. Phys. Med. Biol. *51*, 1479–1489. https://doi.org/10.1088/0031-9155/51/6/008.

65. Ding, H., Lu, J.Q., Jacobs, K.M., and Hu, X.-H. (2005). Determination of refractive indices of porcine skin tissues and Intralipid at eight wavelengths between 325 and 1557 nm. J. Opt. Soc. Am. A *22*, 1151–1157. https://doi.org/10.1364/JOSAA.22.001151.

66. Molina-Borja, M., Font, E., and Mesa Avila, G. (2006). Sex and population variation in ultraviolet reflectance of colour patches in *Gallotia galloti* (Fam. Lacertidae) from Tenerife (Canary Islands). J. Zool. *268*, 193–206. https://doi.org/10.1111/j.1469-7998.2005.00008.x.

67. Bajer, K., Molnár, O., Török, J., and Herczeg, G. (2010). Female European green lizards (*Lacerta viridis*) prefer males with high ultraviolet throat reflectance. Behav. Ecol. Sociobiol. *64*, 2007–2014. https://doi.org/10.1007/s00265-010-1012-2.

68. Olsson, M., Andersson, S., and Wapstra, E. (2011). UV-Deprived Coloration Reduces Success in Mate Acquisition in Male Sand Lizards (*Lacerta agilis*). PLoS One *6*, e19360. https://doi.org/10.1371/journal.pone.0019360.

69. Badiane, A., and Font, E. (2021). Information content of ultraviolet-reflecting colour patches and visual perception of body coloration in the Tyrrhenian wall lizard *Podarcis tiliguerta*. Behav. Ecol. Sociobiol. *75*, 96. https://doi.org/10.1007/s00265-021-03023-2.

70. R Core Team (2025). R: A Language and Environment for Statistical Computing (R Foundation for Statistical Computing).

71. Maia, R., Eliason, C.M., Bitton, P., Doucet, S.M., and Shawkey, M.D. (2013). pavo: an R package for the analysis, visualization and organization of spectral data. Methods Ecol. Evol. *4*, 906–913. https://doi.org/10.1111/2041-210X.12069.

72. Maia, R., Gruson, H., Endler, J.A., and White, T.E. (2019). pavo 2: New tools for the spectral and spatial analysis of colour in r. Methods Ecol. Evol. *10*, 1097–1107. https://doi.org/10.1111/2041-210X.13174.

73. Rasband, W.S. (1997). ImageJ (US National Institutes of Health).

74. Montgomerie, R. (2006). Analyzing colors. In Bird coloration. Mechanisms and measurements, *1*, G.E. Hill and K.J. McGraw, eds. (Cambridge, MA: Harvard University Press), pp. 90–147.

75. Badiane, A., Carazo, P., and Font, E. (2018). Colouration in male blue-throated keeled lizards (*Algyroides nigropunctatus*): Evidence for ultraviolet reflectance of throat and lateral patches. Herpetol. J. *28*, 39–42.

76. Britton, G., Liaaen-Jensen, S., and Pfander, H. (2004). Carotenoids:Handbook (Springer Science & Business Media).

77. Merlin, J.C. (1985). Resonance Raman spectroscopy of carotenoids and carotenoid-containing systems. Pure Appl. Chem. *57*, 785–792. https://doi.org/10.1351/pac198557050785.

78. Moudříková, Š., Nedbal, L., Solovchenko, A., and Mojzeš, P. (2017). Raman microscopy shows that nitrogen-rich cellular inclusions in microalgae are microcrystalline guanine. Algal Res. *23*, 216–222. https://doi.org/10.1016/j.algal.2017.02.009.

79. Hsu, S.L., Moore, W.H., and Krimm, S. (1976). Vibrational spectrum of the unordered polypeptide chain: A Raman study of feather keratin. Biopolymers *15*, 1513–1528. https://doi.org/10.1002/bip.1976.360150807.

80. Galván, I., Jorge, A., Ito, K., Tabuchi, K., Solano, F., and Wakamatsu, K. (2013). Raman spectroscopy as a non-invasive technique for the quantification of melanins in feathers and hairs. Pigment Cell Melanoma Res. *26*, 917–923. https://doi.org/10.1111/pcmr.12140.

81. Morrison, R.L. (1995). A Transmission Electron Microscopic (TEM) Method for Determining Structural Colors Reflected by Lizard Iridophores. Pigment. Cell Res. *8*, 28–36. https://doi.org/10.1111/j.1600-0749.1995.tb00771.x.

82. Johnsen, S. (2011). The Optics of Life: A Biologist's Guide to Light in Nature, 1st ed. (Princeton University Press). https://doi.org/10.23943/princeton/9780691139906.001.0001.

83. Choy, T.C. (2015). Effective Medium Theory: Principles and Applications (Oxford University Press).

84. Land, M.F. (1972). The physics and biology of animal reflectors. Prog. Biophys. Mol. Biol. *24*, 75–106. https://doi.org/10.1016/0079-6107(72)90004-1.

85. Emerson, L.C., Williams, M.W., Tang, I., Hamm, R.N., and Arakawa, E.T. (1975). Optical Properties of Guanine from 2 to 82 eV. Radiat. Res. *63*, 235–244. https://doi.org/10.2307/3574149.

86. Pérez i de Lanuza, G., Carazo, P., and Font, E. (2014). Colours of quality: structural (but not pigment) coloration informs about male quality in a polychromatic lizard. Anim. Behav. *90*, 73–81. https://doi.org/10.1016/j.anbehav.2014.01.017.

87. Martin, M., Le Galliard, J.-F., Meylan, S., and Loew, E.R. (2014). The importance of ultraviolet and near infrared wavelength sensitivity for visual discrimination in two species of lacertid lizards. J. Exp. Biol. *218*, 458–465. https://doi.org/10.1242/jeb.115923.

STAR★METHODS

KEY RESOURCES TABLE

REAGENT or RESOURCE	SOURCE	IDENTIFIER
Biological samples		
Podarcis muralis skin	Natural population in Pyrenees, Spain	N/A
Deposited data		
Raw TEM images of investigated tissues	This manuscript	Brejcha et al.[32] https://doi.org/10.17632/d95wywzjd7.2
TEM images used to measure color producing elements (CPE)	This manuscript	Brejcha et al.[32] https://doi.org/10.17632/d95wywzjd7.2
Measured CPE dimensions	This manuscript	Brejcha et al.[32] https://doi.org/10.17632/d95wywzjd7.2
Raman microscopy data	This manuscript	Brejcha et al.[32] https://doi.org/10.17632/d95wywzjd7.2
Modeled spectra	This manuscript	Brejcha et al.[32] https://doi.org/10.17632/d95wywzjd7.2
Software and algorithms		
OceanView 2.0.14	Ocean Optics	https://www.oceanoptics.com/software/
WITec Project FIVE Plus 5.1	WITec	https://raman.oxinst.com/products/software/suite-seven
R 4.2.2	R Core Team[70]	https://cran.r-project.org/
PAVO	Maia et al.[71,72]	https://pavo.colrverse.com/
ImageJ 1.54p	Rasband[73]	https://imagej.net/ij/

EXPERIMENTAL MODEL AND STUDY PARTICIPANT

Animal handling and treatment

In 2017 eleven adult males of *P. muralis* were captured by noosing in eastern Pyrenees near Puigcerdà (42.43 N, 1.92 E WGS84), and transported to the Ethology Laboratory, Cavanilles Institute of Biodiversity and Evolutionary Biology (University of Valencia), where they were kept for several days in terraria equipped with shelters, a water dish, clean substrate, and artificial UV-enriched lights set to mimic their natural photoperiod. Animals were provided with water *ad libitum* and fed *Tenebrio molitor* larvae every second day. Lizards were anesthetized using Halothane (Sigma Aldrich) and, after no signs of sensitivity were evident, euthanized with an overdose of ketamine HCl (KETOLAR, Pfizer). Immediately after sacrifice, pieces of ventral, dorsal and ventrolateral (including the UV-blue patches) skin were excised, and placed in fixative (see below). For pigment analyses, we used five additional lizards of the same population from previous projects that had been preserved frozen for several years. Permits for sampling and sacrificing all lizards were provided by the Servei de Biodiversitat i Protecció dels Animals, Generalitat de Catalunya (permits SF/474 and SF698). Individuals of the other species, *P. liolepis* (six males captured, but only one used for experiments) and *P. pityusensis* (three males captured, two used for experiments) were captured by noosing in Godella and Dénia respectively (Valencian Community) under Permit no. FAU22_020 and treated the same as individuals of *P. muralis*. All procedures were conducted in accordance with the animal experimentation and care guidelines of the ABS/ASAB and received the approval of the institutional Ethics Committee of the University of Valencia (cod: 2018/VSC/PEA/0127).

METHOD DETAILS

Color measurements and photography

To quantify color, we took reflectance spectra of lizard skin before euthanasia with a USB-2000 portable diode-array spectrometer and a PX-2 xenon strobe light source (all Ocean Optics), and a laptop (Lenovo Legion) running OceanView software (Ocean Optics). The internal trigger was set to 30 (device-specific timing index), integration time to 30 ms, scans average to 20 (unitless), and boxcar width to 10 (unitless). The system was calibrated using a Spectralon WS-1 white diffuse reflectance standard, also from Ocean Optics. Reflectance spectra were taken in a darkened room using a hand-held probe oriented perpendicular to the skin surface (i.e., coincident normal measuring geometry[74]; Montgomerie 2006). An entomological pin (with acrylic head down) attached to the side of the probe allowed us to maintain a fixed 5 mm distance between the probe and the skin surface. To obtain pictures of the skin

in both UV and visible light we used a modified digital camera (Olympus PEN) as described in Badiane et al.[75] High magnification images of the ventrolateral regions were taken through a Leica Macroscope Z16 APO equipped with a DFC 500 digital camera.

Light microscopy

Pieces of dissected skin of ca. 1 cm^2 were briefly fixed in 4% formaldehyde. Following this, samples were washed in phosphate buffer (v/v 1:1–0.2 M PB in deionized water) and transferred to 10% sucrose (1 g sucrose in 10 mL 0.2 M PB) for 1 h, 20% sucrose solution for 1 h, and to 30% sucrose solution overnight before freezing at −20°C. Unstained samples were embedded in Tissue Freezing Medium (Leica) and cut to 15 μm thick sections using a cryotome (Cryocut 1800, Leica). Sections were then observed under bright field illumination with a Nikon Eclipse E800 microscope to assess natural colors of the tissue. To excite autofluorescence of the carotenoid vesicles we used a blue diode (CoolLED's pE-300) and the FITC-3540C filter set (i.e., 482/35 nm excitation and 536/40 nm emission filters) on the same microscope. Further, to test for the presence of lipids in the tissue, we stained cryo-sectioned tissues with Sudan black B. Briefly, cryosections on slides were fixed with Baker's fixative, dehydrated in propylene glycol, stained with Sudan black, differentiated in 85% propylene glycol, washed in water, coverslipped using glycerogel as mounting medium, and observed under the microscope.

Electron microscopy

We subjected skin samples from a total of 11 adult *Podarcis muralis*, one *P. liolepis*, and two *P. pityusensis* individuals to TEM analysis. Altogether, we examined 22 scales containing a UV–sblue patch, and for several of these we prepared ultrathin sections at multiple levels to assess tissue variability. In addition, we sectioned one UV–blue patch skin longitudinally. Fragments of dissected skin of ca. 1 cm^2 were placed in Karnovsky's fixative (2% paraformaldehyde, 2.5% glutaraldehyde, in PB buffer), kept overnight at room temperature, and placed in 4°C for an additional day. Pieces of tissue were observed and photographed using a Leica binocular scope to maintain orientation during the embedding-microscopy process. Smaller pieces of tissue of ca. 2 mm^2 were removed for transmission electron microscopy (TEM) analyses and kept for one week in PB. Samples were washed with 0.1 M PB, postfixed with 2% osmium (in 0.1 M PB solution), washed with 2% uranyl acetate in 70% ethanol solution, dehydrated in an increasing ethanol series, washed in propylene-oxide solution, and embedded in resin (Durcupan, Sigma). One sample was not stained with uranyl acetate to prevent dissolving guanine crystals in the tissues. Resin blocks were cut on an ultramicrotome (Leica UCT Ultracut) to obtain semi-thin sections and ultra-thin sections. Semi-thin sections were stained with toluidine blue and inspected by Nikon Eclipse E800 microscope in bright field to determine the region of interest for the ultra-thin sectioning. Ultra-thin sections were observed and photographed on FEI Tecnai Spirit G2 TEM (Thermo Fisher Scientific) with digital camera (Soft Image System, Morada) using image capture software TIA 4.7SP3. Magnification ranged from 1250× to 43000× depending on structures observed. We quantified the size of 4,929 carotenoid vesicles from epidermal xanthophores using segmented TEM images and the *analyze particles* function in ImageJ.[73] For iridophores, we selected TEM micrographs in which most reflecting platelets were intact, manually outlined them, and measured the thickness of 411 S-iridophore platelets and 607 D-iridophore platelets as the height of the segmented objects using *analyze particles* in ImageJ. Differences in platelet thickness between S- and D-iridophores were evaluated using a generalized linear model, function *glm*, in R.[70]

Pigment analyses

Skin from five frozen specimens was used for pigment analyses. Pieces of skin spanning the whole ventrolateral region, including UV-blue patches, were removed, cleaned of surrounding tissue mechanically with scalpel and tweezers, and washed briefly with PB to get rid of potential contamination from muscles and body fluids. As previous analyses suggested the presence of carotenoids, samples were extracted with 0.5 mL ethyl acetate.[35] The vials with samples in extraction solution were stored for 7 days at room temperature in complete darkness. The extracts were then evaporated to dryness by a stream of nitrogen at 27°C and, immediately prior to the analyses, samples were diluted in ethyl acetate (EtOAc). Characteristic absorbance spectra of carotenoid pigments were determined using a UPLC system Dionex Ultimate 3000 (Thermo Fischer, USA) coupled with a photodiode array (PDA) detector. The separation was performed on Kinetex C18 RP column (2.6 μm, 150 × 2.1 mm; Phenomenex, USA) maintained at 35°C using acetonitrile (A), methanol/water 1:1 v/v (B) and a mixture of *tert*-Butyl methyl ether/acetonitrile/methanol - 86:86:8 v/v/v (C) as mobile phases for gradient elution with constant flow rate 0.2 mL/min. Chromatograms were monitored at 445 and 472 nm. Pigments were identified by comparison with published absorbance spectra.[76]

Small ca. 1 cm^2 pieces of skin containing UV-blue patches were measured using a confocal Raman microscope (WITec alpha300 RSA, WITec, Germany) equipped with 50× EC Epiplan-Neofluar, NA = 0.55 (Zeiss, Germany) objective. A 647 nm Kr^+ laser excitation with a power of ca. 1 mW at the focus plane was used. To obtain Raman map we performed multiple Raman measurements with a scanning step of 200 nm in both directions, voxel size of ca. 1 μm^3 and an integration time of 70 ms per voxel. Data were analyzed using WITec Project FIVE Plus v5.1 software (WITec, Germany) that included multiple steps such as cosmic ray removal, background subtraction, cropping of the spectral edges affected by detector margins, spectral unmixing with the True Component Analysis tool (WITec Project FIVE Plus v5.1), and averaging of the mean spectrum, summing multiple measurements to optimize the signal-to-noise ratio. To confirm the carotenoid Raman spectra, we compared them to spectra of previously detected carotenoids.[77,78] The keratin, guanine, and melanin spectra were confirmed based on comparison with published data.[78–80] Additionally, we acquired reference spectra from analytical standards of: Guanine, Bioultra; β-carotene, Synthetic; Melanin from *Sepia officinalis* (all Merck);

Astaxanthin, Synthetic reference standard (USP); Lutein (PhytoLab). As a reference for keratin we used known keratin materials, specifically a white feather of domestic goose and the shed sheath of a cat claw (Figures S4 and S5).

Modeling of color production

We first identify individual CPEs in the tissue. For each of them, we then follow a traditional method for modeling vertebrate color production by considering one medium, each CPE type, dispersed inside another medium, such as the intracellular matrix.[5,23,45,81] The optical responses of different types of CPEs can then be combined while considering the overall organization of the tissue.[48]

The choice of the optical model for individual CPEs depends primarily on their size relative to the wavelength (λ) of incident light.[82] For CPE sizes $\ll \lambda$, effective medium approach[83] can be used while geometrical or ray optics[36] is relevant in the limit of CPE size $\gg \lambda$ due to less significant interference effects.[22] In our particular case of lizard xanthophores and iridophores, however, the CPE sizes are found to be comparable to λ and neither of the above approaches is applicable. We therefore apply approximative models which consider both wave interference and geometrical description of light propagation.

Our model of lizard skin color production is based on a consideration of three different CPEs stacked in distinct layers: epidermal xanthophore-like cells with their carotenoid vesicles closest to the light source, and the two types of dermal iridophores with their reflecting platelets below (see Figure 3). The xanthophores are considered to be a layer responsible for light scattering and absorption and the underlying iridophores behave like mirrors selective in wavelength. Possible light scattering by the iridophores is beyond the scope of this paper. We then recognize four possible light traces (depicted in Figure S9) if the skin is irradiated by a bright light source. The first two paths (denoted as 1 and 2 in Figure S9) are scattered before or after the interaction with iridophores and are perceived by an observer in a wide range of observation angles (scattering probability by xanthophores is, according to our calculations, much less than 100%, thus it is reasonable to neglect multiple scattering paths). Third path (B in Figure S9) is directly back-scattered on the xanthophore layer. But because our calculations show that the back-scattering of xanthophores is inefficient, we neglect this path completely. Fourth path (denoted as M in Figure S9) does not experience any scattering by xanthophores and undergoes only very efficient mirror-like reflections by iridophores. Compared to the paths 1 and 2, the path M delivers much higher light intensity to the observer because it lacks the scattering event, moreover it is highly directional and thus results in the observation of a saturated specular highlight (small bright and colorless spot). For this reason, the model of coloration of UV-blue patch is restricted to paths 1 and 2. Because a substantial component of the model built on light paths 1 and 2 is also (forward-) scattering by xanthophores, we denote this model as "scatterers model" in the following. Conversely, a model in which xanthophores are regarded as only conventional spectral filters without any ability of efficient light scattering, light follows the path M and the model will be denoted as a "filter model".

To describe the spectrum quantitatively, we define the wavelength-dependent light intensity $I_1(\lambda)$ of the light in path 1. Within our optical model, we assume that CPEs are organized in a single layer, effectively covering a relative surface area S. Incident light is either forward-scattered, back-scattered, absorbed or transmitted with efficiencies $SQ_s, SQ_b \approx 0, SQ_a$ and $[1 - S(Q_s + Q_a)]$, respectively. Note that all these parameters are wavelength-dependent. Reflectances of the superficial and deep iridophore layer will be denoted as R_s and R_d, respectively, their transmittances are hence $T_s = 1 - R_s$ and $T_d = 1 - R_d$. The overall iridophore reflection is combined from an infinite series of paths which is composed of multiple scatterings between the iridophore layers. Note that multiple reflections have to be considered here because of a potentially high reflectance of iridophores, exceeding 50% (cf. Figure 8C). All reflections or passage through the respective layers are then accounted for by assuming a reflectance or a transmittance coefficient multiplying the incident light intensity. For path 1, we get in total:

$$I_1 = SQ_sR_S(1 - S(Q_S + Q_a))I_0 + SQ_S(1 - R_S)R_d(1 - R_S)(1 - S(Q_S + Q_a))I_0 + \ldots$$

$$= SQ_sR_s(1 - S(Q_s + Q_a))\frac{R_s + R_d - 2R_sR_d}{1 - R_sR_d} I_0,$$

where I_0 is the incident light intensity. Note that all parameters in the above expression are wavelength dependent. The xantophore-related terms are calculated using the Mie scattering model of randomly distributed spherical carotenoid vesicles (see Figure S8 for more details on the justification of the Mie scattering model) of epidermal xanthophores and the iridophore parameters stem from a calculation of Bragg reflection from regular stacks of guanine crystals in superficial and deep iridophores. Construction of the spectrum of path 2 is similar and yields the same result $I_2 = I_1$.

In contrast to the color production according to paths 1 and 2 described above, we also evaluate light intensity I_f using a "filter model" where the xanthophores act as spectral filters due to contained pigments.[5,21,48] Passage of light through an absorbing pigment layer of thickness L leads to its transmittance $T_f = \exp[-4\pi \,\mathrm{Im}(N_S)/\lambda]$ according to the Lambert-Beer law, where N_S is the pigment refractive index. Replacing the scattering xantophores by the filtering layer and considering the M path of the reflected light, filter model yields the reflected intensity:

$$I_f = T_f^2 \frac{R_s + R_d - 2R_sR_d}{1 - R_sR_d} I_0.$$

To model the optical properties of dermal iridophores, we considered their CPEs (i.e., the reflecting platelets) as forming a layered medium that interacts with light through Bragg reflection. This occurs when alternating layers of guanine and cytoplasm create constructive interference at specific wavelengths, producing structural color. However, biological multilayer systems often exhibit local perturbations, causing deviations from the ideal reflectance spectra of perfectly periodic structures. To assess the optical contribution of iridophores, we relied on TEM-based measurements of reflecting platelets and on pixel-resolved quantification of crystal and gap thicknesses (see Figure S7). In these analyses, individual crystals were manually outlined to capture their true dimensions, and, assuming light incidence from above, crystal and gap thicknesses were quantified for each column of pixels in the calibrated TEM micrographs and compiled into statistical distributions. The reflecting platelets, composed of guanine with high refractive index ($N = 1.83$[84,85]), form multilayer structures with a high degree of order, allowing us to treat the system as approximately periodic and to consider multiple reflections in the models. The number of layers contributing to light reflection in an iridophore was estimated from wider-field TEM images, yielding 26 ± 5 layers for S-iridophores and 15 ± 3 layers for D-iridophores.

To estimate the reflectance of the iridophores, we applied the transfer matrix method. Rather than using exact measurements from TEM images, we generated a large set ($n = 10^5$) of randomized multilayer stacks with geometrical parameters (crystal thicknesses and their distances) drawn from a typical iridophore cross-section (for additional description of the method see Figure S7). The final reflectance for each iridophore type was obtained by averaging across the simulated data.

To model the optical properties of epidermal xanthophores, we applied Mie theory, as TEM measurements (see above and results section) of their CPEs (i.e., the carotenoid vesicles) are similar in size to the wavelength of visible light. The vesicle size follows the log-normal distribution:

$$P(r) = \frac{1}{wr\sqrt{2\pi}}\exp\left[-\frac{(\log r - \log r_0)^2}{2w^2}\right],$$

where r is the vesicle radius, and $r_0 = 210$ nm and w = 0.43 are the fitted parameters. The optical parameters Q_s and Q_a relevant for our model are hence evaluated by averaging of analytical calculations over the above distribution function. We modeled the vesicles as regular spheres with a (complex) refractive index $N_s(\lambda)$ and used Mie theory[36] to compute their scattering efficiencies. The refractive index was defined as $N_s(\lambda) = N_0 + N'(\lambda) + \frac{i\alpha\lambda A(\lambda)}{4\pi}$ where λ is the wavelength, intrinsic refractive index N_0 is a variable constant, i is the imaginary unit, $A(\lambda)$ is absorption spectrum of β-carotene normalized to peak value equal to 1, α is a variable peak absorption coefficient and $N'(\lambda)$ is wavelength-dependent real part conjugate to the imaginary term through Kramers-Kronig relations. We considered the real constant part N_0 ranging from 1.53 to 1.63, and the values of peak absorption α were considered within a reasonable range, applicable for dilute β-carotene. Even though the vesicles are not distributed randomly within the epidermis volume but are rather aggregated within separate cells, we verified that the description in terms of individual spheres is appropriate as discussed in Figure S8. It is important to stress out that the nonzero imaginary part of the medium inside the xantophore cells expresses their wavelength-dependent optical absorption whose effect is proportional to the peak absorption coefficient α. Xantophores therefore act as spectral filters for light which passes through but the light is in addition considered to be scattered during the interaction.

Visual modeling

Previous attempts to model lizard skin color production as an interaction between the dermal chromatophores have considered xanthophores as mere absorptive spectral "filters" based on their pigment contents[5,21,48] whose theoretical response is expressed by reflected light intensity $I_f(\lambda)$ defined above. In contrast, here we treat xanthophore contents as "scatterers" based on the interaction of the absorptive properties of pigment with geometric properties of the CPEs containing the pigment, giving the perceived light intensity $2I_1(\lambda)$ discussed above.

To test whether the newly proposed mechanism of color production gives a good fit to real spectra of the UV-blue patches in *Podarcis* lizards we simulated three sets of theoretical spectra ("filter" model vs. "scatterers" model, and spectra to simulate tissue mosaicity), and conducted visual modeling based on known properties of the lizard visual system to compare with the real data. The theoretical spectra were simulated considering six levels of relative carotenoid pigment concentration (0, 20, 40, 60, 80, 100%) and using four additional parameters that were common to both color-producing mechanisms: abundance of xanthophores (10, 20, 30, 35, and 40%), abundance of the two types of iridophores (S- and D-) (25, 50, 75, and 100%). The two modeling approaches differed in a fourth parameter that in the case of the "filter" model represents the thickness of the xanthophore layer as proposed previously[48] (200, 420, 700, 1000, 2000, and 2920 nm), while in the "scatterers" model corresponds to the radius of the carotenoid vesicles (100, 210, 350, 500, 1000, and 1460 nm). Thus, in the "filter" models, the effect of the xanthophore is transmission of the pigment layer, while the "scatterers" models consider the effects of xanthophores as an interplay between absorbance due to pigment contents and related scattering extinction. All used parameters vary around measured values from microscopy.

The modeled spectra and measured reflectance spectra of the UV-blue patches acquired from published data[86] were projected into tetrahedral color space based on cone excitation data for *P. muralis*.[87] All the following analyses were performed in R.[70] The tetrahedral color space was based on this visual model using functions *vismodel* and *colspace* from package PAVO.[71,72] Using *vismodel*, we transformed the processed reflectance spectra into predicted photoreceptor stimulation values based on a chosen visual system model. Using *colspace,* we projected the visual model output into a tetrahedral colorspace to quantify and visualize the chromatic relationships among samples. The data were plotted using function *tcsplot* from the same package. To test which of the two

models (“filter” or “scatterers”) better fits the real spectral variability, we compared the modeled spectra with empirical data using the *voloverlap* function from the PAVO package. This function calculates the proportion of one dataset’s color volume that overlaps with another, providing a measure of how well the modeled spectra match the range of observed spectral variation. A higher overlap value indicates a closer correspondence between the simulated and real data, allowing us to assess which color production mechanism better explains the observed UV-blue coloration in *Podarcis* lizards. For each comparison, we report three quantities: the absolute convex-hull volume occupied by each dataset, and two proportional overlap metrics, vsmallest and vboth. Absolute convex-hull volumes quantify the total extent of color space occupied by each dataset, whereas overlap is expressed as proportional overlap using two metrics returned by voloverlap: vsmallest, defined as the fraction of the smaller of the two compared volumes that is shared (containment), and vboth, defined as the fraction of the total volume occupied by both datasets that is shared (overall similarity).

Finally, we simulated the effect of tissue mosaicity, as microscopy data revealed that individual cell types are not homogeneously distributed across the color patches but instead form a mosaic-like arrangement. This heterogeneity may influence measured reflectance spectra, as hand-held spectrophotometers integrate light reflected from approximately 1-2 mm^2 of tissue. To account for this, we modeled how different proportions of S-iridophores, epidermal xanthophores, and D-iridophores contribute to the overall spectral output. We simulated spectra for a gradient of cell-type abundances, with S-iridophores and xanthophores ranging from 100% to 0% cover in 20% increments, while D-iridophores showed the opposite trend, increasing from 0% to 100% in corresponding steps. Using R, the resulting spectra were then projected into tetrahedral color space using same procedures in PAVO mentioned above to examine how mosaic effects influence the occupied regions of color space.

QUANTIFICATION AND STATISTICAL ANALYSIS

All statistical analyses were conducted in R.[70] Details of sample sizes, statistical tests, and quantitative outputs are reported in the figure legends and Results section.

Quantification of subcellular structures

Carotenoid vesicle size was quantified from TEM segmented images using the *analyze particles* function in ImageJ.[73] In total, n = 4,929 vesicles from epidermal xanthophores were measured; here, n represents individual vesicles from multiple sections of different individuals. Vesicle radii were fitted to a log-normal distribution to parameterize Mie scattering models.

For dermal iridophores, platelet thickness was quantified by manually outlining individual crystals in calibrated TEM micrographs. We measured n = 411 platelets from superficial iridophores and n = 607 platelets from deep iridophores; n represents individual crystals. Mean values and dispersion are provided in Figure 8.

Statistical comparison of S- and D-iridophore platelets

Differences in platelet thickness between superficial and deep iridophores were evaluated using a generalized linear model with platelet type as the fixed factor using function *glm* in R. Model outputs (estimate, SE, test statistic, and p-value) are reported in the Results. Assumptions were checked by visual inspection of residuals.

Optical modeling and spectral simulations

Optical models (Mie scattering for xanthophores; transfer-matrix multilayer reflectance for iridophores) were implemented using parameter values obtained from microscopy measurements. Simulated spectra were generated across a range of biologically realistic parameter combinations; no statistical testing was applied to these simulations.

Visual modeling and comparison with empirical spectra

Theoretical and empirical reflectance spectra were projected into tetrahedral color space using the functions *vismodel*, *colspace*, and *tcsplot* in the PAVO package.[71,72] To compare modeled and measured color variation, we used *voloverlap*, which quantifies the proportion of color-space volume shared between datasets. Higher overlap values indicate closer correspondence.

Sample size determination, randomization, and exclusion criteria

No statistical methods were used to predetermine sample sizes; sample sizes reflect availability of specimens. All successfully processed samples were included; no animals or measurements were excluded. Randomization or stratification was not applicable, as individuals were assigned to procedures based on tissue type and methodological requirements.

Definition of central tendency and significance

Unless otherwise stated, data are presented as means. Statistical significance was defined at $\alpha = 0.05$.